JACS
JOURNAL OF THE AMERICAN CHEMICAL SOCIETY
pubs.acs.org/JACS
Article

Carbon–Nitrogen Bond Formation Using Sodium Hexamethyldisilazide: Solvent-Dependent Reactivities and Mechanisms

Qiulin You and David B. Collum*

Cite This: https://doi.org/10.1021/jacs.3c07317
Read Online

ABSTRACT: The solvent-dependent reactivity of sodium hexamethyldisilazide (NaHMDS) toward carbon-centered electrophiles reveals reactions that are poorly represented or unrepresented in the literature, including direct aminolysis of aromatic methyl esters to give carboxamides, nitriles, or amidines, depending on the choice of solvent. S_NAr substitutions of aryl halides and opening of terminal epoxides are also examined. A combination of ^1H and ^{29}Si nuclear magnetic resonance (NMR) spectroscopic studies using [^{15}N]NaHMDS, kinetic studies, and computational studies reveals the complex mechanistic basis of the preferences for simple aryl carboxamides in toluene and dimethylethylamine and arylnitriles or amidines in tetrahydrofuran (THF). A prevalence of dimer- and mixed dimer-based chemistry even starting from the observable NaHMDS monomer in THF solution is notable.

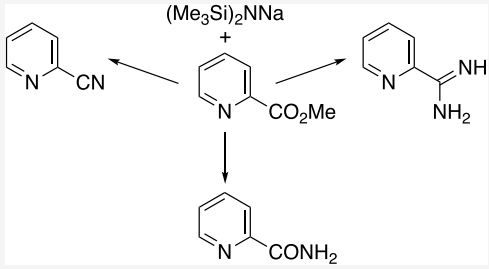

■ INTRODUCTION

After decades of communal disinterest in organosodium chemistry, we began trying to shine a light on its potential by expanding the toolbox for generating and using organosodium species.[1−3] This involved some minor adjustments to protocols for generating and handling sodium diisopropylamide (NaDA)[2,3] as well as developing a new reagent, sodium isopropyl(trimethyl)silyl amide (NaPTA), that manifests desirable solubilities and reactivities as a strong base.[4] Our primary approach, however, is decidedly structural and mechanistic with the faith that understanding how solvation and aggregation influence reactivity and selectivity will propel applications through a combination of serendipity in our laboratory and need-driven progress by others. Even the most prominent organosodium reagent, sodium hexamethyldisilazide (NaHMDS),[5] while garnering the attention of crystallographers,[6] had evaded spectroscopic, mechanistic, and computational scrutiny until recent studies of its solvent-dependent structure and reactivity toward enolization.[7]

This brings us to the current work. Aminolyses illustrated with generic examples in Scheme 1 are legion. S_NAr substitutions and peptide bond formations are of unquestioned importance in pharmaceutical chemistry.[8,9] With that said, any reaction in which the electrophile is merely heated in ammonia or simple alkylamine will be difficult to improve upon. However, should these simple protocols fail, owing to low reactivity or poor selectivity, the experimentalist is left with few options. In these instances, metal amides could offer solutions through the control of their coordination spheres.

We describe herein a survey of the reactivity of NaHMDS toward carbon-centered electrophiles of potential interest in synthesis, accompanied by detailed structural and mechanistic studies. NaHMDS plays the role of a highly reactive analogue of ammonia and a preface to expanding investigations of sodium alkylsilazides.[4] Some of the transformations surveyed as opportunities for mechanistic studies piqued our interest as synthetically promising and have surprisingly little or no presence in the NaHMDS literature. The more mechanistically inclined will find the prevalence of dimer- and mixed aggregate-based reactivity surprising.[10] We also inadvertently stumbled into the complex world of organosilicon chemistry.

Scheme 1. Generic Aminolyses

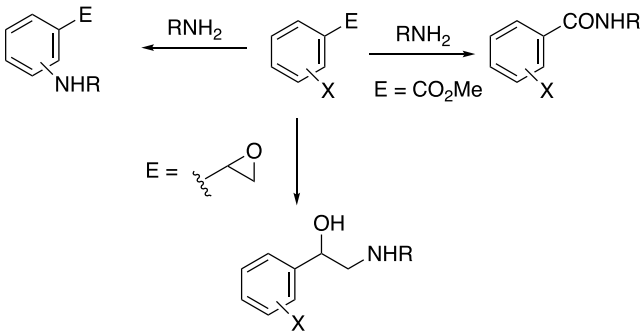

Received: July 10, 2023

Table 1. Reactions of NaHMDS with Electrophiles in Various Solvents

entry	substrate	conditions	product	yield
1	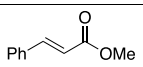 **1**	2.0 equiv NaHMDS 25 °C, 5 h toluene	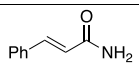 **2**	72%
2	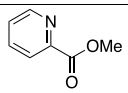 **3**	3.0 equiv NaHMDS 25 °C, 0.3 h DMEA	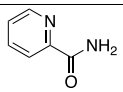 **4**	95%
3	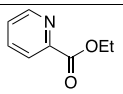 **5**	3.0 equiv NaHMDS 25 °C, 0.3 h toluene	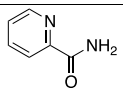 **4**	90%
4	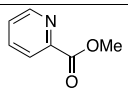 **3**	1.0 equiv NaHMDS 50 °C, 1.0 h THF	 **6**	86%
5	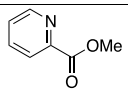 **3**	3.0 equiv NaHMDS 50 °C, 0.3 h THF	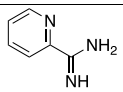 **7**	92%
6	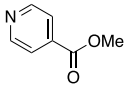 **8**	3.0 equiv NaHMDS 70 °C, 0.3 h toluene[a]	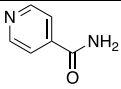 **9**	85%
7	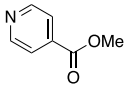 **8**	3.0 equiv NaHMDS 70 °C, 1.0 h THF	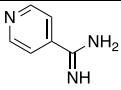 **10**	96%
8	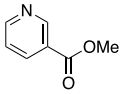 **11**	2.0 equiv NaHMDS 70 °C, 1.0 h toluene	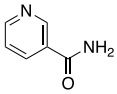 **12**	76%
9	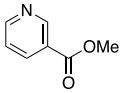 **11**	3.0 equiv NaHMDS 70 °C, 1.0 h THF	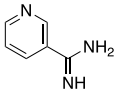 **13**	95%
10	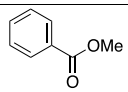 **14**	3.0 equiv NaHMDS 50 °C, 1 h DMEA	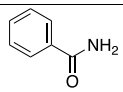 **15**	78%
11	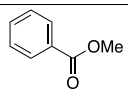 **14**	3.0 equiv NaHMDS/ THF 70 °C, 2.0 h 25 °C, 24 h	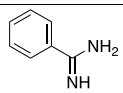 **16**	92%
12	 **17**	2.0 equiv NaHMDS 25 °C, 0.05 h DMEA	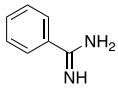 **16**	95%
13	 **18**	2.0 equiv NaHMDS 25 °C, 2 h toluene	 **19**	85%
14	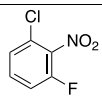 **20**	2.0 equiv NaHMDS 25 °C, 1.0 h toluene	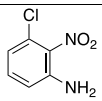 **21**	77%
15	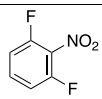 **22**	2.0 equiv NaHMDS 25 °C, 1.0 h toluene	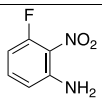 **23**	83%
16	 **24**	2.0 equiv NaHMDS 110 °C, 2 h toluene	 **25**	55%
17	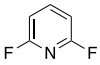 **26**	2.0 equiv NaHMDS 110 °C, 3 h toluene	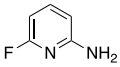 **27**	76%
18	 **28**	2.0 equiv NaHMDS 60 °C, 24 h toluene	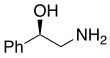 (>50:1) **29**	86%
19	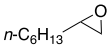 **30**	2.0 equiv NaHMDS 25 °C, 24 h THF	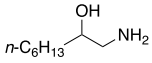 **31**	76%

[a]Forms a gel-like mixture during the reaction.

■ RESULTS AND DISCUSSION

Aminolyses. Substitutions of representative organic substrates by NaHMDS are summarized in Table 1. The yields are of isolated, purified products that have been desilylated during workup. ^{1}H and ^{29}Si NMR spectroscopic monitoring (vide infra) shows the reactions are often pristine and reveals unisolated silylated and sodiated intermediates. The times and temperatures listed in Table 1 are those required to achieve high conversion, as confirmed by in situ monitoring using NMR or IR spectroscopies.

For context, the aminolysis of methyl cinnamate to form carboxamide (entry 1) rather than alternatives such as 1,4-addition,[11,12] enolization,[5] or generalized destruction caught our attention. Ester aminolyses by LiHMDS and NaHMDS may populate pharmaceutical notebooks, but they are poorly represented in the published literature. In 1963, Krüger et al. aminolyzed an aryl ester with NaHMDS to form an O-methyloximino ether, an intermediate en route to carboxamides (as in entry 2). One is detected in mechanistic studies below.[13] In 1998, Hwu and co-workers reported a NaHMDS-mediated conversion of aryl esters to nitriles with NaHMDS at 110−185 °C (as in entry 4), attributing a central importance to phenolic groups.[14] One-pot conversions of aryl esters to amidines (entries 11 and 12) or carboxamides (such as entry

https://doi.org/10.1021/jacs.3c07317
J. Am. Chem. Soc. XXXX, XXX, XXX−XXX

2) by NaHMDS are unreported. Additions to nitriles to form amidinates (as in entry 12) are well-known for LiHMDS.[15] Mechanistic studies below offer some thoughts on why analogous additions of NaHMDS to nitriles are rare.[16]

The potentially useful selectivities for the formation of carboxamides, nitriles, and amidines directly from esters have complex mechanistic underpinnings dependent on the solvent, temperature, and equivalents of NaHMDS (vide infra). The 3- and 4-picoline methyl esters form gels in weak solvents (entries 9 and 11), presumably owing to head-to-tail oligomeric substrate-NaHMDS dimer complexes but without negative consequences.

S_NAr reactions (entries 15−19) represent a reaction class of unquestioned importance.[8] We find it somewhat confounding that the S_NAr reactions seem to be more effective with soft nucleophiles. Malonates, for example, are far superior nucleophiles[17] than unstabilized enolates.[18] We can find only one report of direct (uncatalyzed) S_NAr substitution by LiHMDS[19] and none for NaHMDS, while RNH_2-based aminolyses *facilitated by* LiHMDS are legion albeit with an unknown role of the LiHMDS.[20] We expended considerable effort trying to glean mechanistic insights (entry 15−17) only to be thwarted by deeply colored debris that appears to be diazo derivatives arising from NaHMDS reacting with the nitro moiety noted years ago (eq 1).[21] Nitroarenes are spartan in the voluminous literature of lithium amide-mediated ortholithiations,[22] possibly for similar reasons.

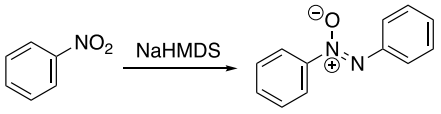

(1)

A few problematic substrates are illustrated in Chart 1. Arenes **32**−**34** gave complex products suggestive of ortho-

Chart 1. Failed and Troublesome Substrates

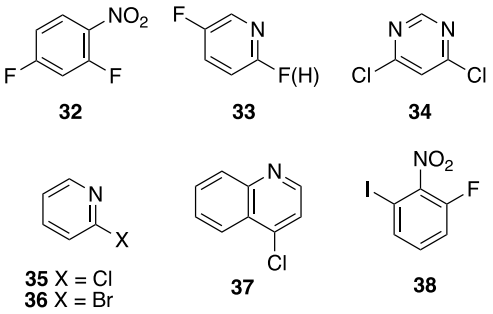

metalations and possibly pyridyne intermediates. Halopyridines **35** and **36** and chloroisoquinoline **37** aminated but were prone to transfer a silyl group to the 3-position by a Fries-like process.[23] Nitrobenzene **38** underwent a clean halogen dance,[24] forming 2-fluoro-3-iodonitrobenzene.[25]

We replicated the highly regioselective epoxide openings reported by Withnall and co-workers in 2008[26] (entries 20 and 21) to evaluate them as candidates for mechanistic work and include these potentially useful results because they have gone largely unnoticed.[27]

To assist the reader, Scheme 2 represents a road map to forthcoming mechanistic studies. We explore the reaction coordinates to convert NaHMDS and methyl picolinate **3** to carboxamide **4** in DMEA (Part 1), to nitrile **6** in THF (Part 2),

Scheme 2. Focus of the Four Studies Examined Spectroscopically, Kinetically, and Computationally

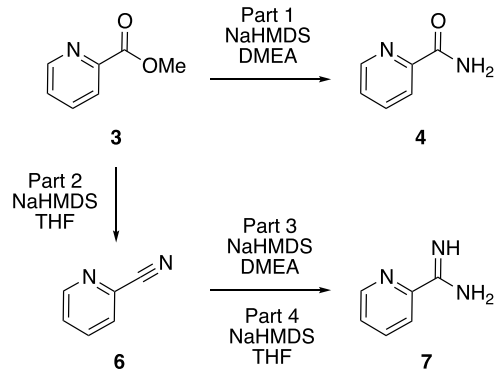

and conversion of nitrile **6** to amidine **7** in DMEA (Part 3) and THF (Part 4). Each part delves into the underlying organosodium and organosilicon chemistry by examining spectroscopically observable structural events, kinetic studies to evaluate solvation and aggregation in the rate-limiting transition structures,[28] and computational probes of solvation, aggregation, critical transition structures, and elusive details along the reaction coordinates.[29,30]

Monitoring the reactions by ^{1}H and ^{29}Si NMR spectroscopies showed that the reactions were very clean and provided detailed structural assignments. [^{15}N]NaHMDS[7] distinguished O−Si and ^{15}N−Si species owing to ^{15}N−^{29}Si coupling, whereas combinations of [^{15}N]NaHMDS and NaHMDS were exploited to examine reversible steps. DFT computations using Me_3N in place of Me_2NEt to reduce unnecessary degrees of freedom revealed an exothermic substitution of DMEA on dimer **39**. We took the liberty of using the original numbers assigned to DMEA solvates in the schemes showing computed Me_3N solvates. The shorthand of the general form A_mS_n alludes to the hexamethyldisilazide fragment (A) and solvent (S).

Part 1: Mechanism of Aminolysis of Methyl-2-Picolinate (3) with NaHMDS/DMEA. We focused on structure−reactivity studies on additions to methyl-2-picolinate in DMEA and THF. Toluene acts similarly to DMEA but affords broader resonances. The reaction coordinate for the addition of NaHMDS to picoline **3** in DMEA observable by NMR spectroscopy is summarized in Scheme 3. Mono- and dichelated dimers **40** and **41** observable at −80 °C reflect the behavior of NaHMDS with other bifunctional ligands studied previously.[7] Both dimers display coupling constants ($^1J_{N-Si}$ = 8.5 and 8.7 Hz, respectively) and chemical shifts (−15.8 and −16.4 ppm, respectively) characteristic of [^{15}N]NaHMDS dimers.[7] Addition of excess **3** affords computationally viable doubly chelated monomer **42** with an upfield ^{29}Si chemical shift and large coupling constant (−21.41 ppm, $^1J_{N-Si}$ = 13.1 Hz) characteristic of a NaHMDS monomer.[7] Rate studies (below) place dimer **40** on the reaction coordinate. The stability of **43** allows carboxamide **4**[31] to be isolated in high yield (Table 1, entry 5).[32]

The computed structure of **40** (Figure 1) reveals a geometry that more closely approximates square planarity than tetrahedral sodium. Serial substitution from **39** to **41** is computed to be mildly exothermic for both steps (ignoring translational entropy).[34] DFT supports monomer stereoisomer **42**, with the alternative stereoisomeric monomer (not drawn) being 10.4 kcal/mol less stable.

https://doi.org/10.1021/jacs.3c07317
J. Am. Chem. Soc. XXXX, XXX, XXX−XXX

Scheme 3. Spectroscopically Observed Species on the Reaction of Methyl-2-Picolinate with NaHMDS/DMEA[33]

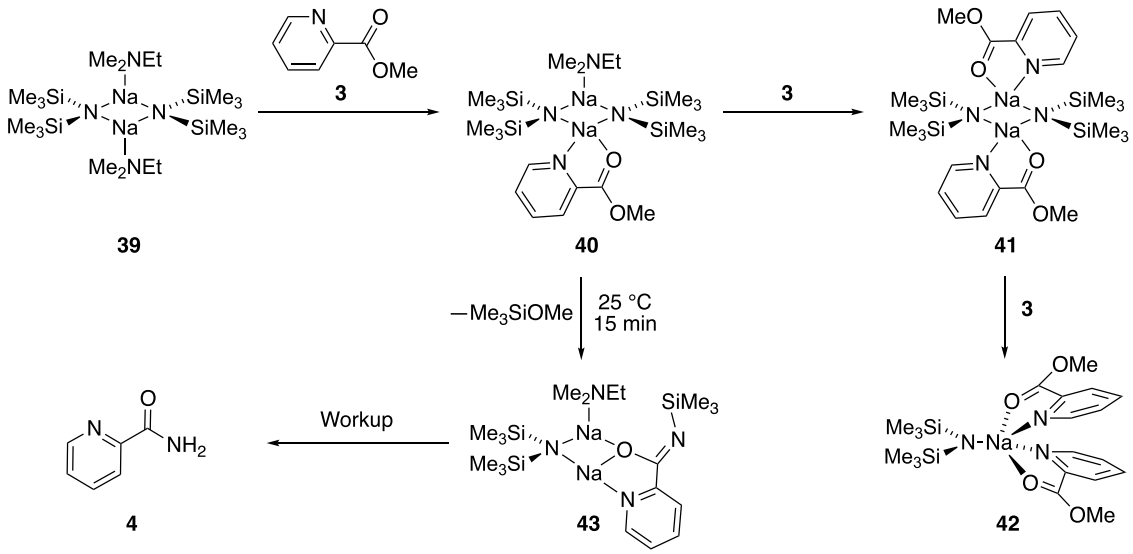

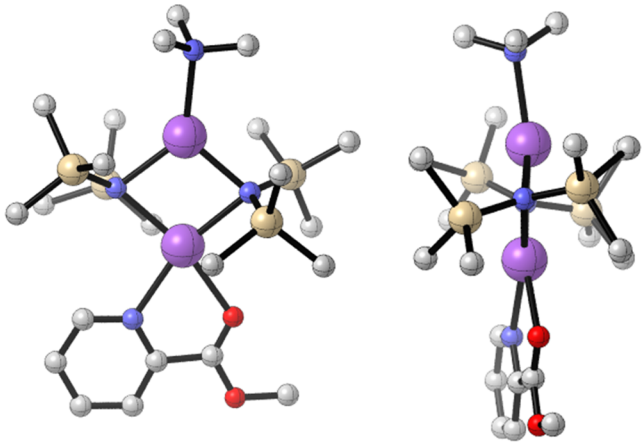

Figure 1. Ball-and-stick depictions of DFT-computed dimer **40** displaying an approximate 10° rotation of the chelate and Na_2N_2 planes from coplanarity.

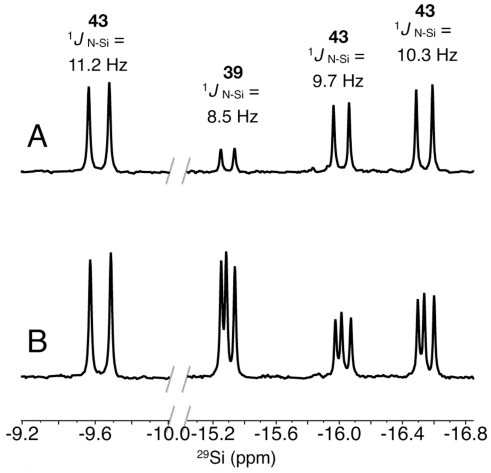

Figure 2. Spectrum A is the ^{29}Si NMR spectrum of 0.05 M ester **3** with 0.10 M added [^{15}N]NaHMDS in DMEA after reaction containing only mixed aggregate [^{15}N]**43** and residual NaHMDS dimer [^{15}N]**39** (Scheme 3). Spectrum B is the sample from spectrum A with 1.0 equiv (relative to ester 3) of unlabeled NaHMDS.

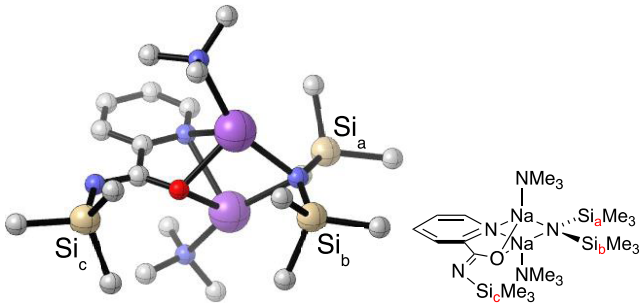

Figure 3. Ball-and-stick depictions of DFT-computed and artist's rendition of mixed aggregate **43** with Me_3N as a DMEA surrogate.

The only observable species during the aminolysis in DMEA are mixed aggregate **43** (Figure 2A) and Me_3SiOMe with the latter confirmed by comparison with an authentic sample (^{29}Si, δ 17.49 ppm). Two ^{29}Si resonances of **43** at −16.0 ppm ($^1J_{N-Si}$ = 9.7 Hz) and −16.6 ppm ($^1J_{N-Si}$ = 10.3 Hz) are similar to those of [^{15}N]NaHMDS dimer **39** (−15.2 ppm, J_{N-Si} = 8.5 Hz) and coalesce into a single broad resonance at −20 °C. The imino ^{29}Si resonance is markedly downfield (−9.70 ppm, J_{N-Si} = 11.2 Hz). Addition of excess unlabeled NaHMDS to preformed [$^{15}N_2$]**43** at −80 °C shows immediate incorporation of unlabeled silazide fragments (Figure 2B). DFT computations illustrate the magnetic inequivalence of the two silazide-derived Me_3Si moieties in **43** (Figure 3).

We probed the mechanism for the addition of NaHMDS to picolinate **3** in DMEA-pentane mixtures using in situ IR spectroscopy[35] under pseudo-first-order conditions (excess NaHMDS) following the loss of monochelated dimer **40** (1737 cm^{-1}) to form mixed dimer **43** (1584 cm^{-1}). Clean first-order decays (Figure 4) afford pseudo-first-order rate constants, k_{obsd}, that are independent of the initial concentration of **40**. Plotting k_{obsd} vs DMEA concentration with pentane cosolvent (Figure 5) and vs NaHMDS dimer **39** concentration (Figure 6) shows zeroth-order dependencies. The resulting rate law (eq 2) is consistent with a rate-limiting addition via a transition structure of the stoichiometry A_2S(substrate). (Recall that A is an amide subunit and S is solvent.) The dimer-based reaction coordinate is a hallmark of

https://doi.org/10.1021/jacs.3c07317
J. Am. Chem. Soc. XXXX, XXX, XXX−XXX

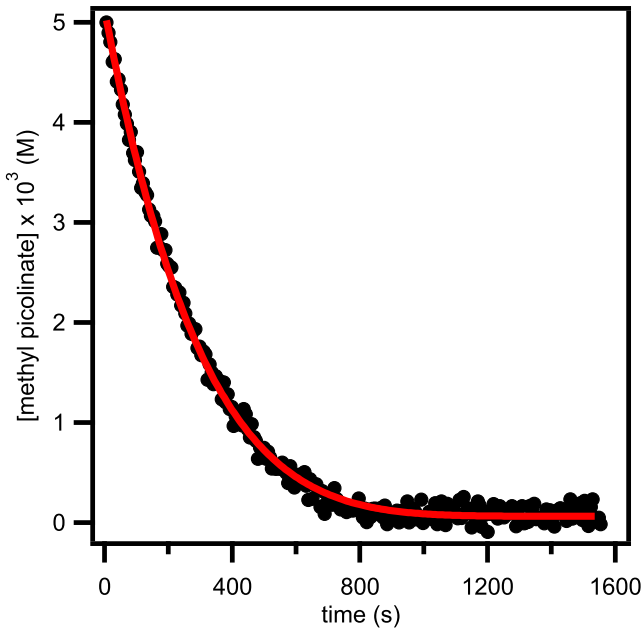

Figure 4. Addition of 0.10 M NaHMDS to methyl-2-picolinate (**3**, 0.005 M) at 25 °C was measured with IR spectroscopy (1737 cm^{-1}). The curve depicts an unweighted least-squares fit to $y = ae^{-bx}$ ($a = 8.1 \times 10^{-3} \pm 0.1 \times 10^{-3}$; $b = 1.5 \times 10^{-3} \pm 0.1 \times 10^{-3}$).

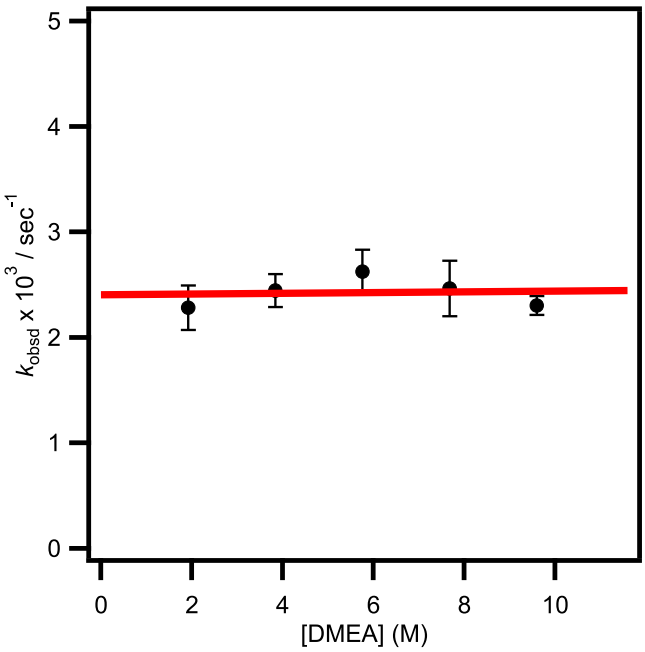

Figure 5. A plot of k_{obsd} vs [DMEA] (M) in pentane for the addition of NaHMDS (0.10 M) to methyl-2-picolinate (**3**, 0.005 M) at 25 °C measured with IR spectroscopy (1737 cm^{-1}). The curve depicts an unweighted least-squares fit to $y = ax + b$ ($a = 2.4 \times 10^{-3} \pm 0.2 \times 10^{-4}$; $b = 3.3 \times 10^{-6} \pm 0.3 \times 10^{-6}$).

alkali metal amides in poorly coordinating solvents.[2,7c,36] Figure 7 depicts the computed transition structure **TS-1** displaying a developing $Na_2(O)(N)$ mixed dimer core.

$$-d[\mathbf{40}]/dt = k'[\mathbf{40}]^1[A_2S_2]^0[S]^0 \quad (2)$$

Probing the reaction coordinate en route to observable product **43** (carboxamide **13** after workup) and Me_3SiOMe

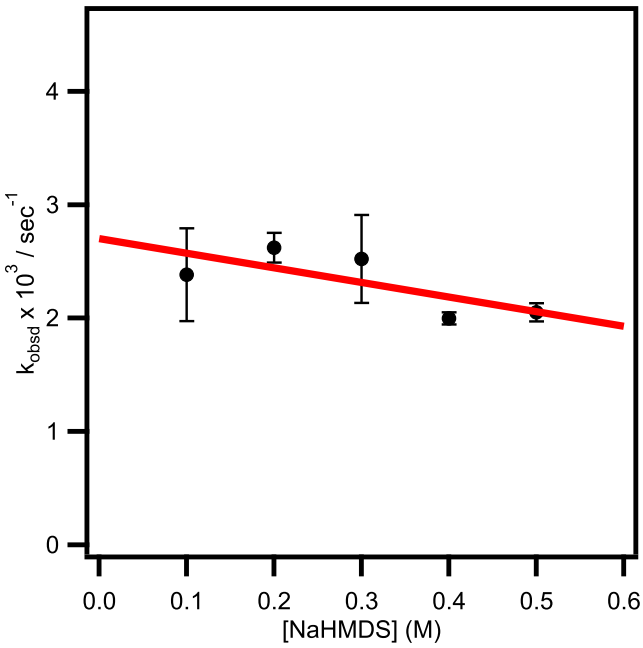

Figure 6. A plot of k_{obsd} vs [NaHMDS] (M) for the addition of NaHMDS to methyl-2-picolinate (**3**, 0.050 M) in 9.6 M (neat) DMEA at 25 °C measured with IR spectroscopy (1737 cm^{-1}). The curve depicts an unweighted least-squares fit to $y = ax + b$ ($a = 2.7 \times 10^{-3} \pm 0.2 \times 10^{-3}$; $b = -1.3 \times 10^{-3} \pm 0.1 \times 10^{-3}$).

using DFT computations served up a nuanced and quite complex story (Scheme 4). To reiterate, Me_3N is used as a surrogate of DMEA to reduce unnecessary degrees of freedom while taking the liberty of reusing the original numbers for **40**, **43**, and **46**. Transition structures **TS-1**, **TS-2**, **TS-3**, and **TS-4** all have single-negative frequencies. Intrinsic reaction coordinate (IRC) calculations[37] were used to determine the minima flanking each transition structure. Minima connected without connecting transition structures represent structural minima corresponding to reorganizations of insufficient interest to probe further. There are likely more minima and barriers resulting from other minor adjustments. These same caveats also apply to the reaction coordinate depicted in Scheme 6 (below).

Following the formation of open dimer **45**,[36] the 1,2-addition proceeds via the rate-limiting transition structure **TS-1** (depicted in Figure 7) to form the tetrahedral adduct as mixed aggregate **46**. Structures beyond **TS-1** represent kinetically and spectroscopically invisible post-rate-limiting events. The collapse of adduct **46** via transition structure **TS-2** affords NaOMe−NaHMDS mixed dimer **47**. Following a readjustment via **TS-3** to position the methoxy as a MeO−Si Lewis acid−base complex **48**, silyl transfer via transition structure **TS-4** extrudes Me_3SiOMe via complex **49** to form mixed dimer **50** (same structure compared to mixed aggregate **43** instead utilizing Me_3N as a solvent surrogate in DFT-computation) as the spectroscopically observable product (albeit with an exothermic addition of a second solvent).

As drawn, the NaOMe silylation is an intra-aggregate reaction. We cannot exclude the possibility that NaOMe is released into solution before silyl transfer, but we have no reason to invoke it either. We also probed for a methoxy-silyl coupling directly from the tetrahedral adduct **46** without first expelling NaOMe (see **51**, path a) but were unable to locate such a transfer. Similarly, a silyl transfer to extrude $NaOSiMe_3$

https://doi.org/10.1021/jacs.3c07317
J. Am. Chem. Soc. XXXX, XXX, XXX−XXX

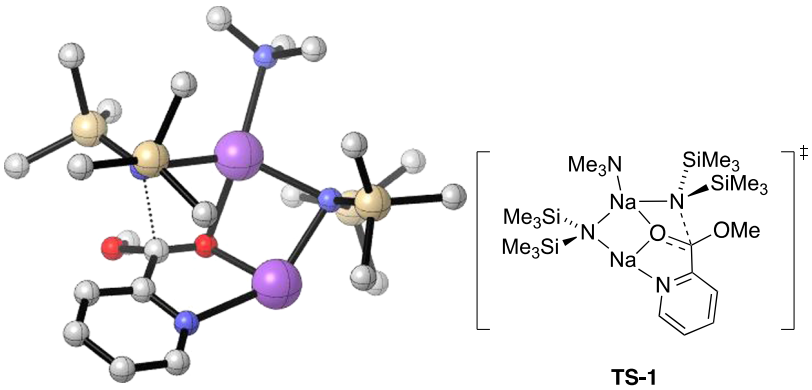

Figure 7. DFT-computed transition structure **TS-1** for NaHMDS-based addition to methyl-2-picolinate (**3**) with Me_3N as a DMEA surrogate.

Scheme 4. DFT-Computed Reaction Coordinate for the Aminolysis of Methyl-2-Picolinate (3) by NaHMDS Using Me_3N as a DMEA Surrogate

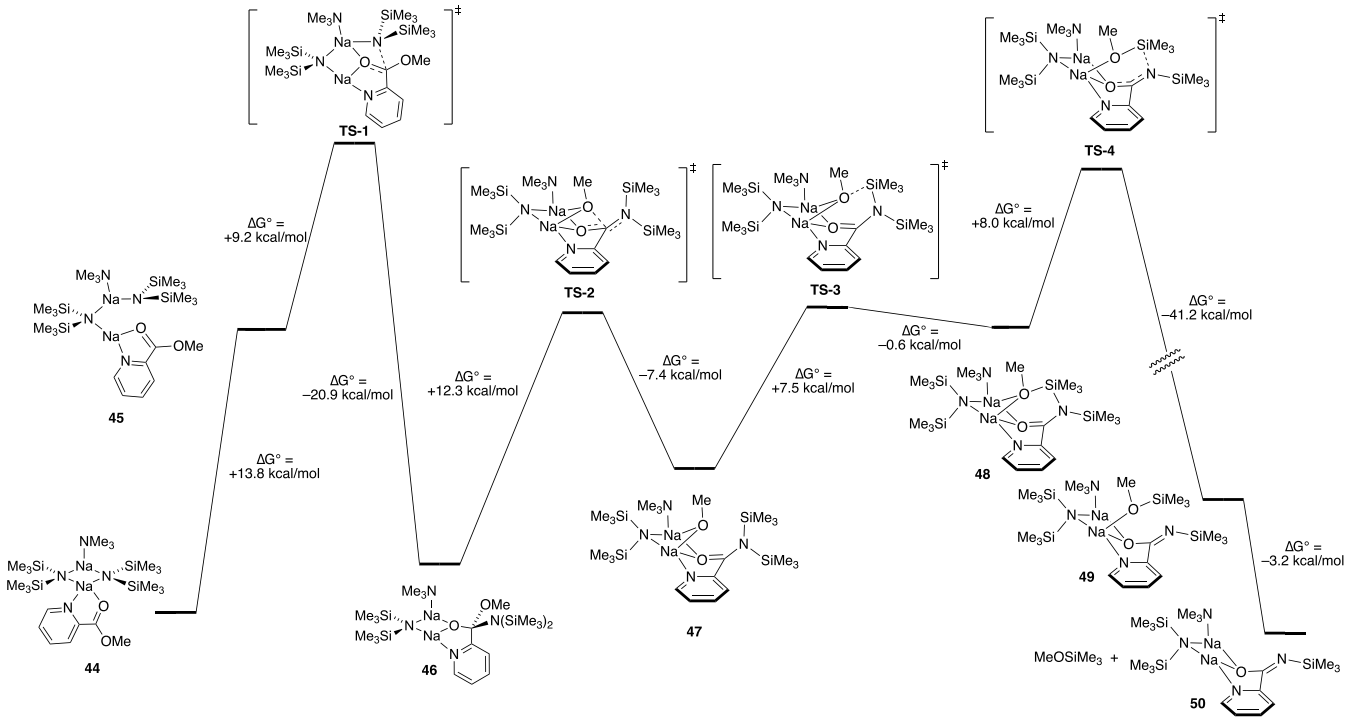

from **46** (see **51**, path b) was located but had an unreasonably high (23 kcal/mol) barrier consistent with our failure to observe Me_3SiONa spectroscopically.

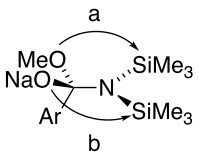

51

Part 2: Mechanism of Aminolysis of Methyl-2-Picolinate (3) with NaHMDS/THF. The aminolysis in THF follows a distinctly different pathway. The spectroscopically observable forms summarized in Scheme 5 show mechanistic complexity lurking beneath the surface. At the outset, we note that the excess NaHMDS undergoes a THF-dependent deaggregation of disolvated dimer **52** to provide tetrasolvated monomer **53** described previously,[7a,b] which proves to be mechanistically important. Picolinate-complexed dimer **54** (analogous to **9**) and THF-complexed monomer **55** can be observed at −110 °C at both low and high THF concentrations, using a pentane cosolvent. Evidence of complexation is gleaned from distinct chemical shift differences in the ^{1}H and ^{29}Si NMR spectra when compared with the uncomplexed substrate **3** and free NaHMDS (Supporting Information). The assigned THF solvation numbers derive from DFT computations.

Warming mixtures of **3** and NaHMDS to room temperature affords imino ether **56**, analogous to that isolated previously,[13] within 1.0 min. The concomitant formation of Me_3SiONa was confirmed by comparison with an authentic sample (17.70 ppm). In the absence of excess NaHMDS, **56** gives nitrile **6** over 24 h at RT or in 30 min at 50 °C in good yield (Table 1, entry 7) with concomitant formation of Me_3SiOMe, confirmed with an authentic sample. The conversion of **56** to **6** is somewhat mysterious in that it does not appear to require NaHMDS and is not accelerated by excess NaHMDS, yet it does not occur by heating a crude isolated sample of **56**.

https://doi.org/10.1021/jacs.3c07317
J. Am. Chem. Soc. XXXX, XXX, XXX−XXX

Scheme 5. Spectroscopically Observed Species for the Reaction of NaHMDS to Methyl-2-Picolinate 3 in THF

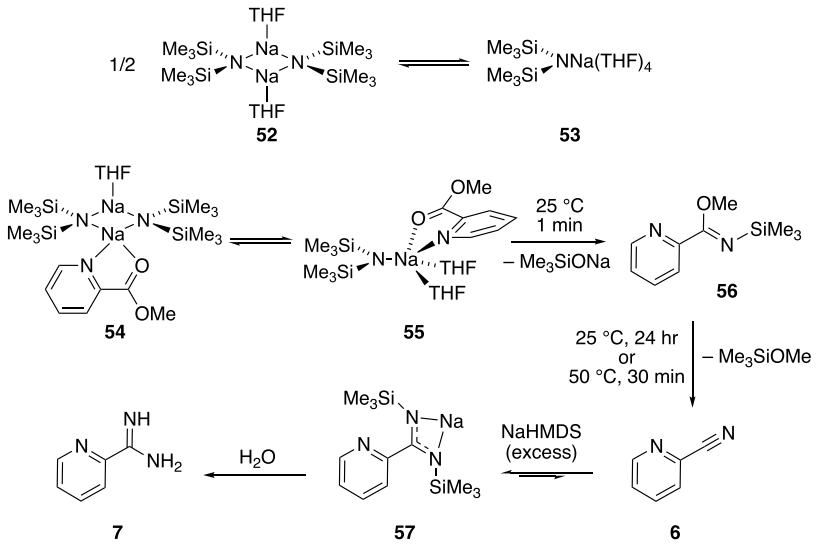

Reaction of **3** with excess NaHMDS renders nitrile **6** unobservable because it is quickly scavenged to give amidinate **57**[38] with noteworthy spectroscopic properties. The ^{29}Si resonance of [^{15}N$_2$]**57** appears as a clean triplet owing to second-order effects referred to as "virtual coupling." The two magnetically equivalent ^{29}Si nuclei experience equivalent coupling by the ^{15}N nuclei despite one being proximal and one being distal to each silicon nucleus (Figure 8). Similar virtual coupling is observed in bridging transition metal phosphides (M_2P_2 core)[39] and has been observed in a Li_2P_2 lithium phosphide dimer.[40] In theory, we could have observed this in NaHMDS (Na_2N_2) dimers as well but have not.[7] If the symmetry is broken by generating [^{15}N$_1$]**57** from unlabeled nitrile **6** and [^{15}N]NaHMDS, the ^{29}Si resonance appears as a doublet of doublets owing to a large $^1J_{N-Si}$ coupling and small $^3J_{N-Si}$ coupling with a slight isotopic perturbation visible.[41]

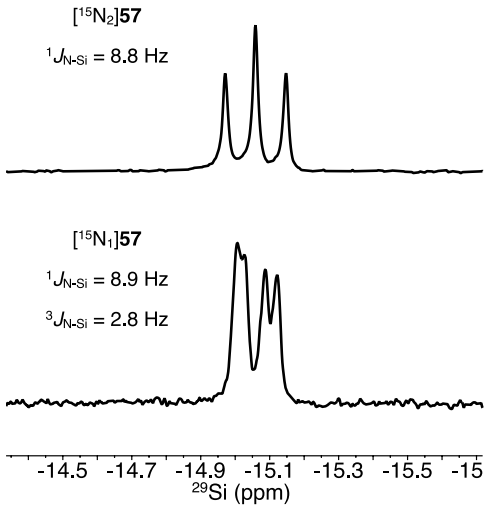

Figure 8. ^{29}Si NMR spectra of [^{15}N$_2$]**57** showing virtual coupling ($^1J_{N-Si}$ = 8.8 Hz) and standard coupling in [^{15}N$_1$]**57** ($^1J_{N-Si}$ = 8.9 Hz and $^3J_{N-Si}$ = 2.8 Hz).

The requisite silyl transfer from initially formed unsymmetric *N,N*-disilylamidine to *N,N′*-disilylamidine **56** is discussed in the context of DFT computations below. The depicted **6**−**57** nitrile-amidinate equilibrium cannot be observed directly, but adding [^{14}N]NaHMDS to labeled amidinate **57** results in label exchange (eq 3).

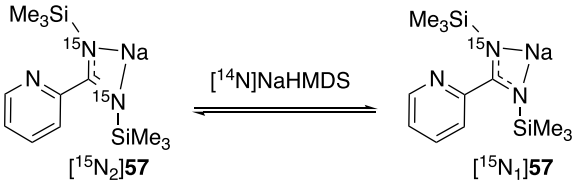

(3)

An analogous addition of NaHMDS to $PhCO_2Me$ (Table 1, entry 13) to generate phenyl-substituted amidinate **58** was approximately 60-fold (see Supporting Information) slower than for **3**. It also revealed the elusive nitrile-amidinate exchange as a temperature-dependent equilibrium (eq 4). Heating excess NaHMDS (3.0 equiv) and $PhCO_2Me$ to 80 °C followed by rapid thermal quenching to −80 °C affords predominantly benzonitrile (**17**). Alternatively, cooling the reaction to 25 °C and letting it stand for 12 h generated amidinate **58**. Heating−cooling cycles show the changes are temperature dependent and reversible. Adding [^{15}N]NaHMDS to unlabeled benzonitrile, **17**, shows label incorporation in both **17** and **58**. Thus, benzonitrile can be isolated in 86% yield using 1.1 equiv of NaHMDS and elevated temperatures (Table 1, entry 13), while amidine **58** can be isolated in 98% yield using 3.0 equiv of NaHMDS at 80 °C for 3 h and then 25 °C for 12 h. This odd temperature dependence in which heating accelerates the aminolysis but retards addition to the intermediate nitrile might be why nitrile-to-amidine conversions largely exploit LiHMDS[15] rather than NaHMDS.[16] Alternatively, it could just be a cultural preference for LiHMDS. There are no extraneous silazide signals in the ^{29}Si spectrum that would implicate a mixed aggregate.

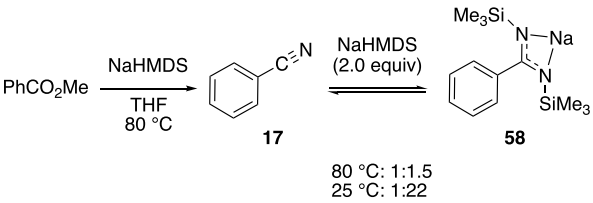

(4)

https://doi.org/10.1021/jacs.3c07317
J. Am. Chem. Soc. XXXX, XXX, XXX−XXX

Rate studies for the addition of NaHMDS to picolinate **3** to afford imino ether **56** provided yet another nuanced story. We anticipated that the first-order dependence—the first-order decay—on complexed monomer **55** measured in neat THF would be accompanied by a zeroth-order NaHMDS dependence. To the contrary, a plot of k_{obsd} vs NaHMDS shows a half-order dependence on the free NaHMDS monomer (Figure 9).

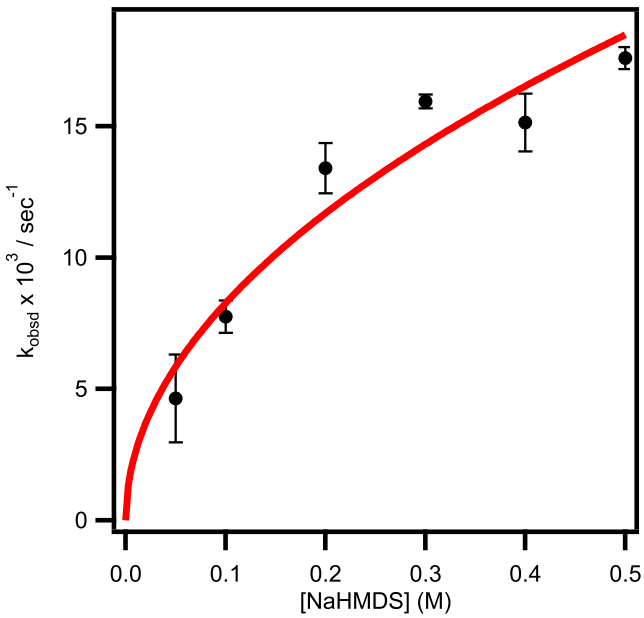

Figure 9. Plot of k_{obsd} vs [NaHMDS] (M) for the addition of NaHMDS to methyl-2-picolinate (**3**, 0.005 M) in 12.8 M (neat) THF at 0 °C measured with IR spectroscopy (1731 cm^{-1}). The curve depicts an unweighted least-squares fit to y = ax^n ($a = 2.4 \times 10^{-3} \pm 0.1 \times 10^{-3}$; $n = 0.44 \pm 0.01$).

The *partial* rate law (deferring discussion of solvent-concentration dependencies momentarily) is described by eq 5. To be clear on a critical point, a dimer-based addition involving contributions of a standard NaHMDS monomer would manifest a first-order NaHMDS dependence.[42] The *half-order* on a monomer demands a full ionization of the sodium cation.[43]

$$-d[\mathbf{55}]/dt = k'[\mathbf{55}]^1[AS_4]^{1/2}$$
$$\text{such that} \quad \mathbf{55} = AS_2(\mathbf{3}) \tag{5}$$

We may not yet fully understand the role of solvation. The forthcoming discussion may even seem excessive, but we are still struggling to understand how organosodium solvation and aggregation differ from those of organolithiums. A plot of k_{obsd} vs THF in pentane (Figure 10, curve A) manifests a maximum in the rates at intermediate THF concentrations. By contrast, analogous data using 2,5-dimethyltetrahydrofuran (2,5-Me_2THF) or the decidedly more expensive 2,2,5,5-tetramethyltetrahydrofuran (2,2,5,5-Me_4THF) as poorly coordinating polar cosolvents[44−47] eliminate the maximum. The solvent dependencies *suggest* that medium effects are in play. We remind the reader that *two* deaggregations are occurring concurrently. At low THF concentrations, the dimeric reactant A_2S(substrate) (**54**) exists concurrently with A_2S_2 (NaHMDS dimer **52**), and the rise in rates indicates they are collectively undersolvated relative to the rate-limiting transition structure.

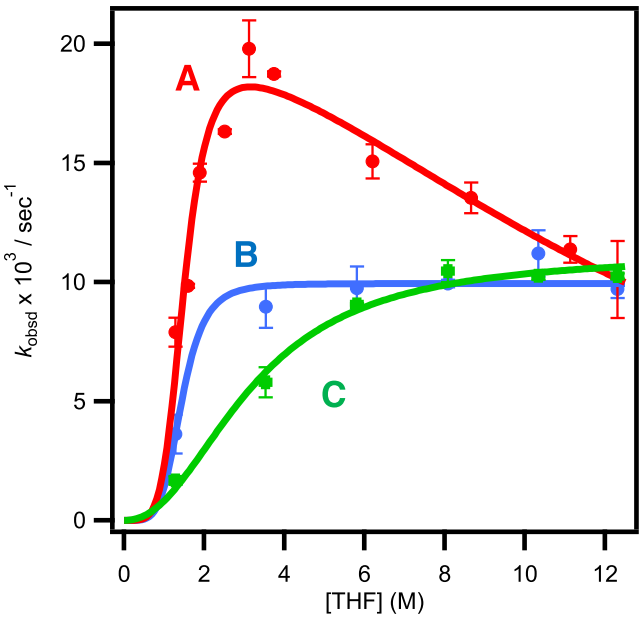

Figure 10. A plot of k_{obsd} vs [THF] (M) for the addition of NaHMDS to methyl-2-picolinate (**3**, 0.005 M) in 0.10 M NaHMDS at 0 °C measured with IR spectroscopy (1732 cm^{-1}). Curve A derives from pentane cosolvent and depicts an unweighted least-squares fit to $y = [ax^n/(1+bx^n)](1/1+cx^2)$ ($a = 2.4 \times 10^{-3} \pm 0.1 \times 10^{-3}$; $b = 1.3 \times 10^{-1} \pm 0.1 \times 10^{-1}$; $c = 0.6 \times 10^{-3} \pm 0.1 \times 10^{-4}$; $n = 5$). Curve B derives from 2,5-Me_2THF cosolvent and depicts an unweighted least-squares fit to $y = ax^n/(1+bx^n)$ ($a = 1.6 \times 10^{-1} \pm 0.1 \times 10^{-1}$; $b = 1.6 \times 10^{-1} \pm 0.1 \times 10^{-1}$; $n = 5$). Curve C derives from 2,2,5,5-Me_4THF cosolvent and depicts an unweighted least-squares fit to $y = ax^n/(1+bx^n)$ ($a = 8.2 \times 10^{-4} \pm 0.1 \times 10^{-1}$; $b = 7.9 \times 10^{-2} \pm 0.1 \times 10^{-2}$; $n = 2.2 \pm 0.2$).

At high THF concentrations in polar cosolvents, the observable reactants AS_2(substrate) (**54**) and AS_4[7c] (**53**) appear optimally solvated − six THF ligands total − but under-aggregated relative to the dimeric rate-limiting transition structure.

The problem we confronted in this study was that 2,5-Me_2THF was binding *cooperatively* with THF to promote monomer formation as illustrated in eq 6. At a low THF concentration, an unusually elevated concentration of NaHMDS monomer in 2,5-Me_2THF compared with pentane implicates a $(Me_3Si)_2N(THF)_x(Me_2THF)_y$ mixed solvate. However, there is almost no chance that 2,2,5,5-Me_4THF cooperatively solvates monomers, and DFT computations support this assertion. We still observe the promotion of the monomer. Thus, the flattening of the curve is at least partially attributable to such an unproductive side equilibrium to form a mixed solvate according to the Principle of Detailed Balance.[48] We must confess that the function used to fit the THF/pentane data (caption in Figure 10) contains a correction for inhibitory medium effects, $1/(1+cx^2)$, that was derived empirically with no formal molecular basis. The challenge posed by these medium effects rears its ugly head below.

With all that said, the rate law in eq 5 provides an adequate picture of a mechanism requiring 6 solvents and two silazide subunits − a hexasolvated dimer-based transition structure **TS-5** (Figure 11) with a $^+Na(THF)_6$ gegenion (Figure 12).[36]

We computationally examined the overall reaction coordinate using a triple-ion-based framework (Scheme 6). The cation (Figure 12) is omitted for all of the structures in Scheme 6. Triple ions are well precedented,[36] including for

https://doi.org/10.1021/jacs.3c07317
J. Am. Chem. Soc. XXXX, XXX, XXX−XXX

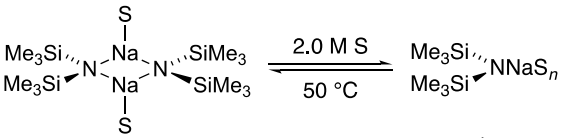

cosolvent, S (°C)	monomer/ dimer
pentane (50 °C)	1 : 23
Me_2THF (50 °C)	1.3 : 1
Me_2THF (−110 °C)	>50 : 1
Me_4THF (50 °C)	1 : 3

LiHMDS. Inspection of Figure 11, however, reveals that it is a triple-ion-based reference state (**59**) because the lowest-energy rate-limiting transition structure **TS-5** has lost all semblance of the N−Na−N triple-ion connectivity as has the IRC-derived minimum **61** preceding it.

There is plenty of room for alternative interpretation. One could, for example, imagine **61** stemming directly from a chelated monomer and ionized NaHMDS fragment. It is also possible, however, that the conversion of **60** to transition structure **TS-5** proceeds via **61** in which the $(Me_3Si)_2N^-$ in **61** remains "bound." (The dissociation of **61** is calculated to be +5.5 kcal/mol) Transition structure **TS-5** gives way to the tetrahedral adduct **62**. The sequence follows an aza-Brook-like silicon transfer akin to that presumed to occur in an aza-Peterson-like imine formation[49] via transition structure **TS-6**, elimination of **63** via transition structure **TS-7** to form arene π complex **64**, and arene dissociation to afford the observed imino ether **56** and unobserved (fleeting) mixed triple-ion **65**.[36,50]

Part 3: Mechanism of Aminolysis of 2-Pyridinecarbonitrile (6) with NaHMDS/DMEA. Motivated as much by an obsessive need to complete the story as by curiosity, we examined the addition of NaHMDS to nitrile **6** to form amidinate **57** (Scheme 5) and were rewarded for our persistence. IR and NMR spectroscopy showed no evidence that nitrile **6** binds to NaHMDS at low or high DMEA concentrations. The addition occurs to give mixed amidinate **66** within seconds at 25 °C (eq 7) manifesting a silazide fragment displaying dimer-like coupling ($^1J_{N-Si}$ = 8.5 Hz; Figure 13) that is well resolved from NaHMDS homodimer **39**. As described above, further heating to 50 °C causes scrambling of the $^{14}N-^{15}N$ isotopes.

Rate studies show an inverse-second-order dependence on DMEA (Figure 14) and first-order dependence on the NaHMDS dimer **39** (Figure 15) consistent with a disolvated-dimer-based 1,2-addition. A full computational workup is found in the Supporting Information. An

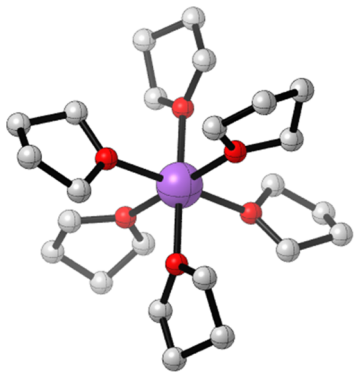

Figure 12. DFT-computed $^+Na(THF)_6$.

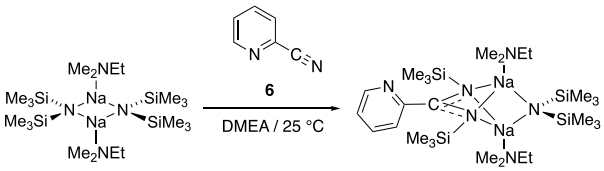

39 66

abbreviated version is illustrated in Scheme 7. For example, the conversion of **70** to **66** requires several additional mundane readjustments. Also, we examined the role of solvation of the intermediates and found minima that were higher energy than the unsolvated forms except for **70**, whose Me_3N-solvated form is a −2.5 kcal/mol more stable.

Part 4. Mechanism of Aminolysis of 2-Pyridinecarbonitrile (6) with NaHMDS/THF. IR and NMR spectroscopy showed no evidence that nitrile **6** binds to NaHMDS (eq 8). The only species observable by ^1H and ^{29}Si NMR spectroscopy was free NaHMDS (**52** and **53**, Scheme 5) and sodium amidinate **57** to the exclusion of any mixed aggregate. DFT computations suggest that **57** is a disolvate.

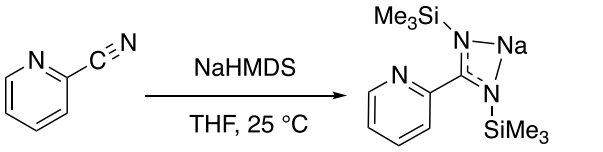

6 57

Rate studies showed first-order decays and concentration-independent values of k_{obsd}, consistent with a first-order dependence on nitrile **6**. A plot of k_{obsd} vs THF concentration

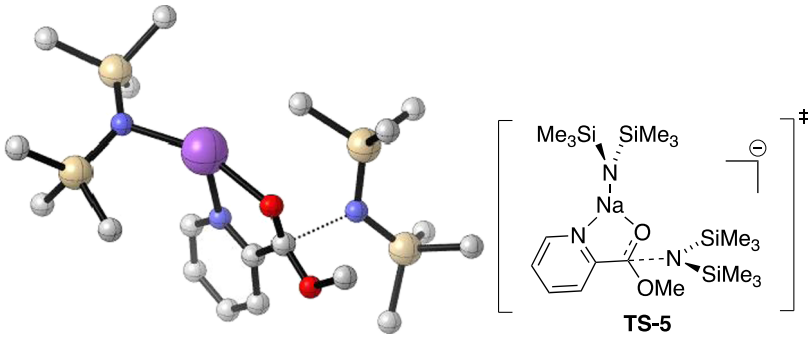

Figure 11. DFT-computed transition structure **TS-5** for the NaHMDS-based addition to methyl-2-picolinate (**3**) solvated by THF. The implicit $^+Na(THF)_6$ cation[7b] (Figure 12) is not included.

https://doi.org/10.1021/jacs.3c07317
J. Am. Chem. Soc. XXXX, XXX, XXX−XXX

Scheme 6. DFT-Computed Reaction Coordinate for the Aminolysis of Methyl-2-Picolinate (3) with NaHMDS in THF with the $^{+}Na(THF)_6$ Omitted for All Structures

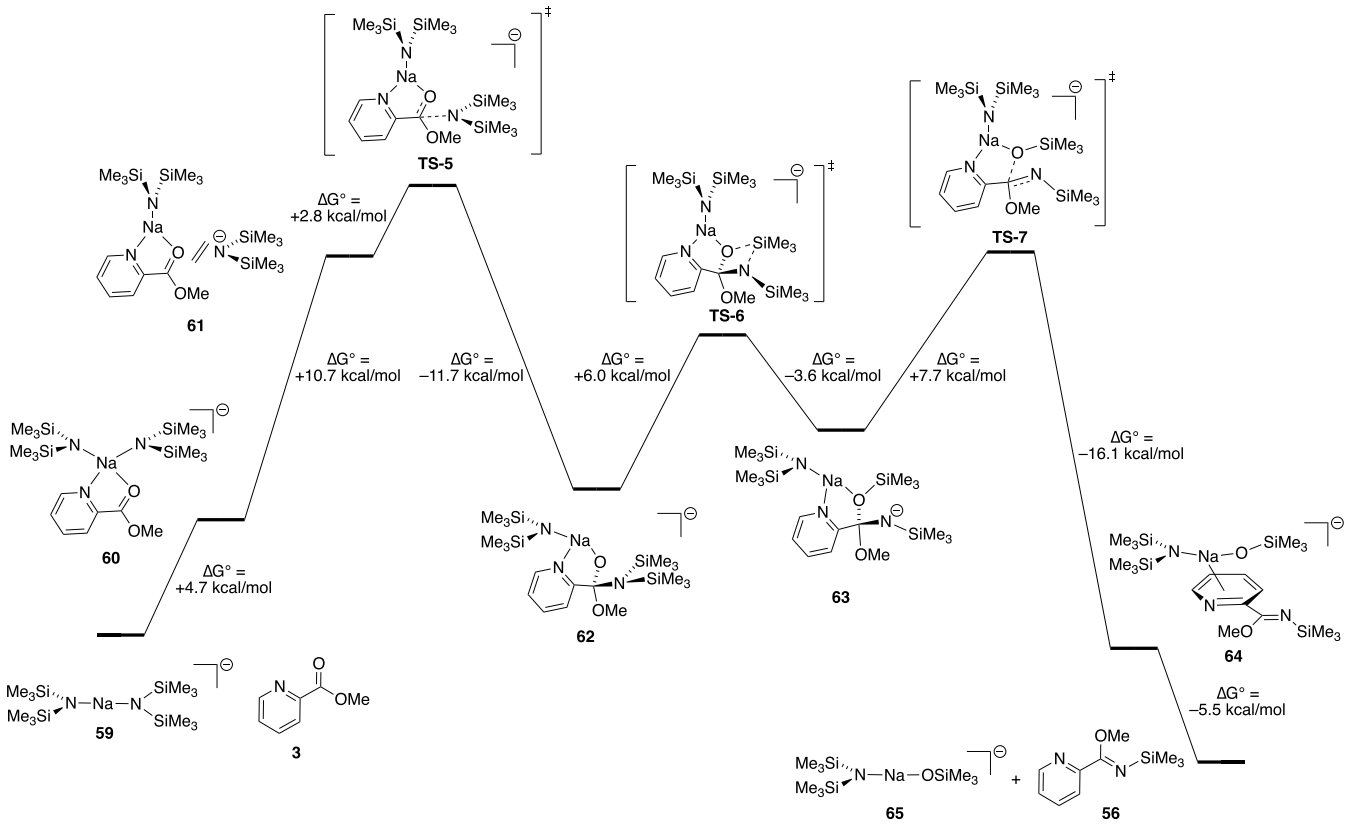

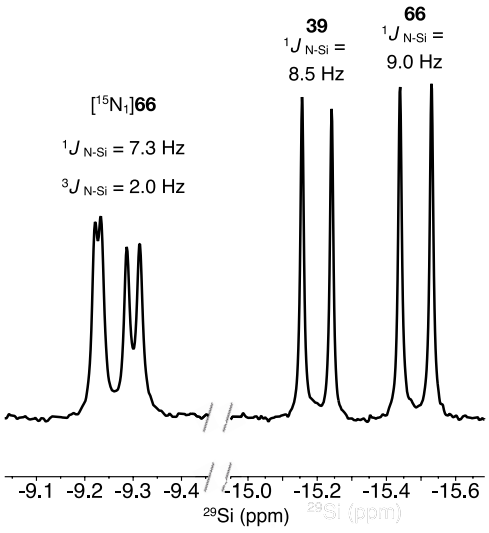

Figure 13. ^{29}Si NMR spectra of the [$^{15}N_2$]NaHMDS dimer (**39**, $^{1}J_{N-Si}$ = 8.5 Hz) and mixed aggregate [$^{15}N_1$]**66** ($^{1}J_{N-Si}$ = 7.3 Hz, $^{3}J_{N-Si}$ = 2.0 Hz).

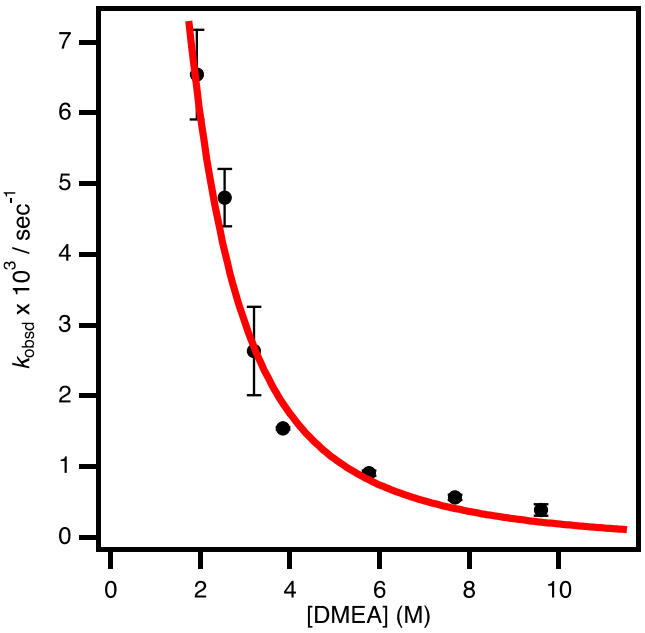

Figure 14. A plot of k_{obsd} vs [DMEA] (M) in pentane for the addition of NaHMDS to pyridinecarbonitrile (**6**, 0.005 M) at −40 °C measured with IR spectroscopy (1584 cm^{-1}). The curve depicts an unweighted least-squares fit to $y = ax^n/(1+bx^n)$ ($n = -1.9 \pm 0.1$; $a = 2.3 \times 10^{-2} \pm 0.1 \times 10^{-2}$; $b = 1.7 \times 10^{-1} \pm 0.1 \times 10^{-1}$).

shows a distinct sigmoidal dependence affording a pronounced inhibition at high THF (Figure 16, curve A). Any doubt that this correlates with the NaHMDS dimer−monomer deaggregation (**52** and **53**, Scheme 5) was put to rest by superimposing the rate data on a plot of the equilibrium population of dimer (curve B) measured in 2020 by a different experimentalist.[7b] Clearly, deaggregation inhibits the reaction. A plot of k_{obsd} vs NaHMDS in *neat* THF where NaHMDS is >98% monomer shows a clean second-order dependence (Figure 17), consistent with a requisite monomer-to-dimer aggregation before rate-limiting addition. The crudely defined zeroth-order THF dependence implicates the *partial* rate law in eq 9, pointing to the overall dimer-based transition

https://doi.org/10.1021/jacs.3c07317
J. Am. Chem. Soc. XXXX, XXX, XXX−XXX

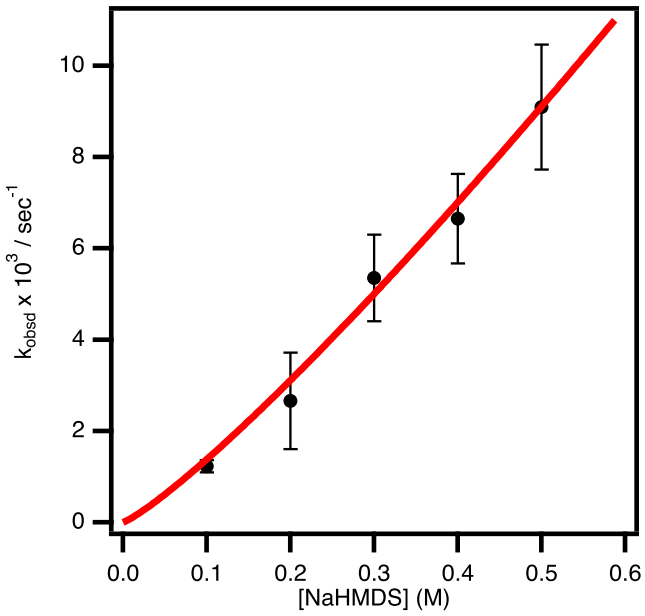

Figure 15. Plot of k_{obsd} vs [NaHMDS] (M) for the addition of NaHMDS to 2-pyridinecarbonitrile (**6**, 0.005 M) in 9.6 M (neat) DMEA at −40 °C measured with IR spectroscopy (1584 cm^{-1}). The curve depicts an unweighted least-squares fit to $y = ax^n$ ($a = 2.1 \times 10^{-2} \pm 0.1 \times 10^{-2}$; $n = 1.1 \pm 0.1$).

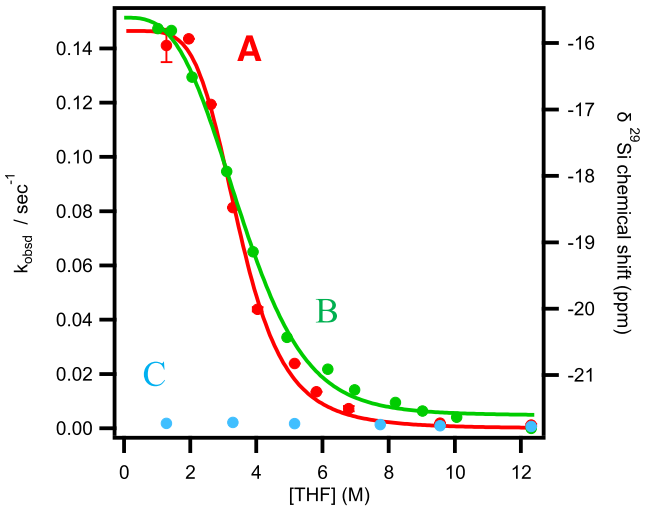

Figure 16. A plot of k_{obsd} vs [THF] (M) for the addition of NaHMDS to 2-pyridinecarbonitrile in pentane cosolvent (curve A, red) and ^{29}Si chemical shift (curve B, green) plotted vs [THF] in 2:1 pentane/toluene as cosolvent measured at −20 °C. The latter function fits to a model based on an A_2S_2−AS_4 equilibrium (Supporting Information).[7b,52] The blue data (Curve C) derive from 2,5-Me_2THF rather than pentane as cosolvent (vide infra).

Scheme 7. DFT-Computed Reaction Coordinate for the Aminolysis of 2-Pyridinecarbonitrile (6) by NaHMDS Using Me_3N as a DMEA Surrogate

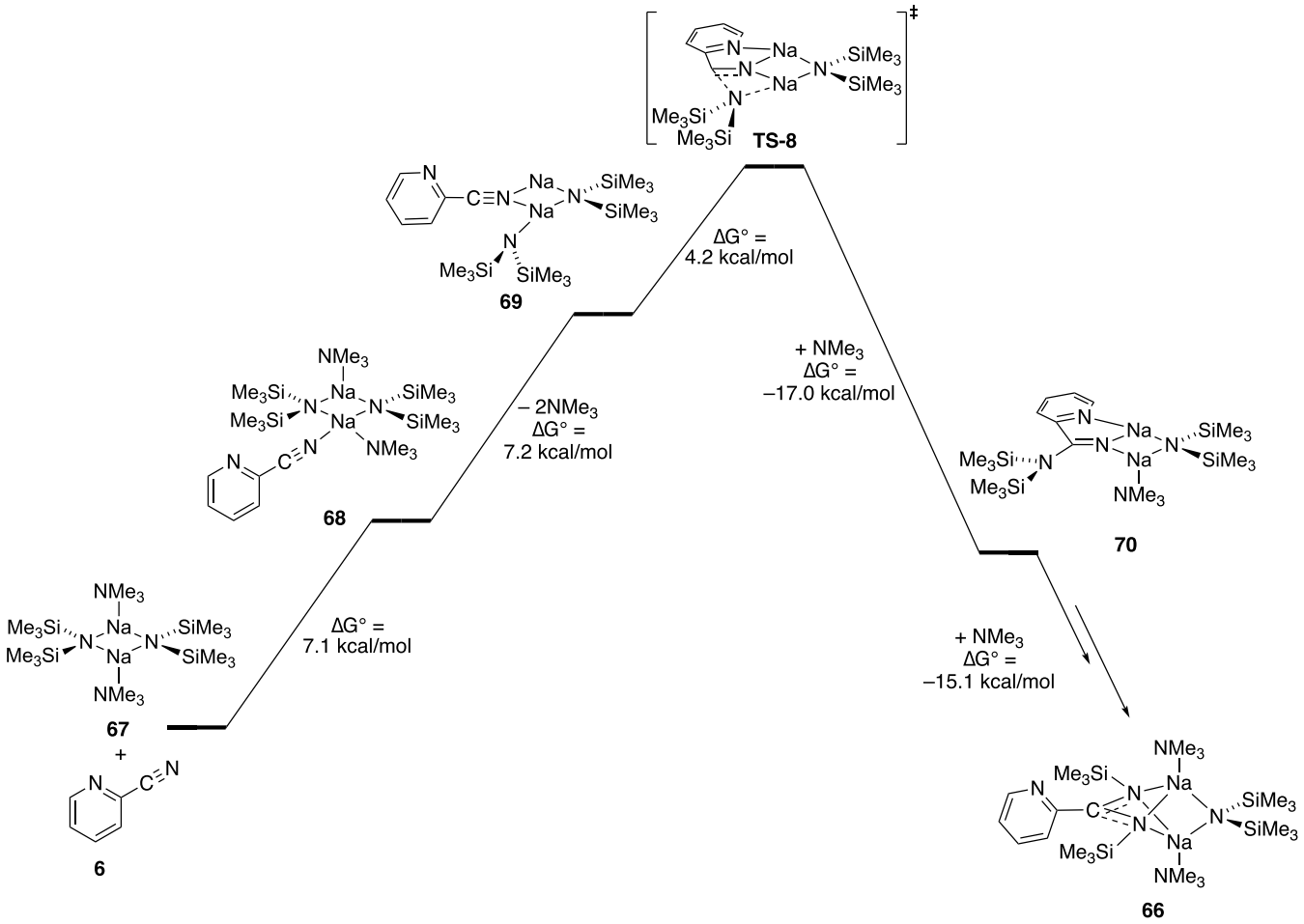

https://doi.org/10.1021/jacs.3c07317
J. Am. Chem. Soc. XXXX, XXX, XXX−XXX

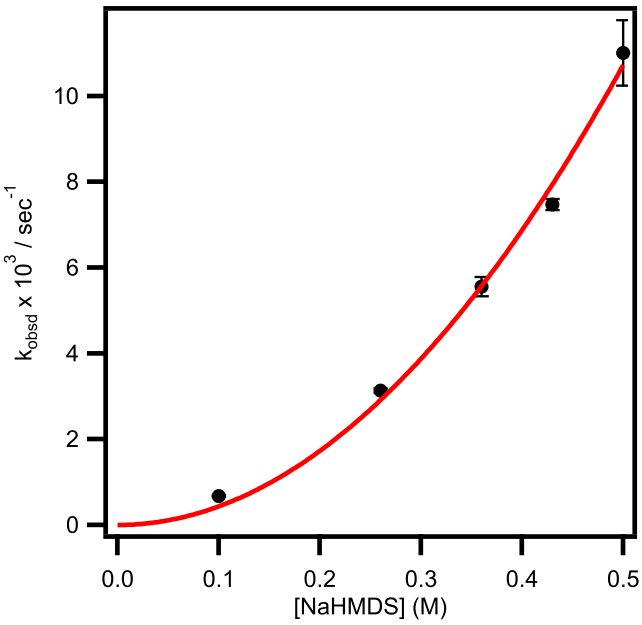

Figure 17. Plot of k_{obsd} vs [NaHMDS] (M) for the addition of NaHMDS to picolinonitrile (**6**, 0.005 M) in 12.8 M (neat) THF at −20 °C measured with IR spectroscopy (1584 cm^{-1}). The curve depicts an unweighted least-squares fit to $y = ax^n$ ($a = 4.3 \times 10^{-2} \pm 0.1 \times 10^{-2}$; $n = 2.0 \pm 0.1$).

structure, $[A_2S_2(ArCN)]^{\ddagger}$.[51,52] The DFT-computed transition structure **TS-10** is illustrated in Figure 18.

$$-d[\mathbf{6}]/dt = k'[\mathbf{6}]^1[AS_4]^2 \quad (9)$$

The DFT-computed reaction coordinate for addition to nitrile **6** in THF shows many parallels with that in DMEA that are relegated to the Supporting Information. The notable differences are the exothermic solvation of all key species including transition structure **TS-10** in Figure 18, mixed dimer-based transition structure **TS-9** for silicon transfer, and unobserved mixed aggregate **71** whose analog (**66**, eq 7) was fully characterized in DMEA.[53]

We have accumulated evidence of preaggregation-based reactions originating from monomers, but none have ever been so poignant.[36] Why is the dimer-based addition to nitriles dominant? A partial answer is that the trajectory of the silazide attack on the nitrile π system in **TS-10** (Figure 18) appears

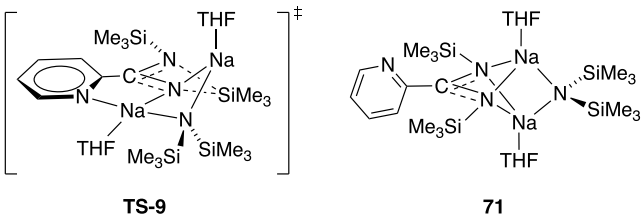

optimal. The most stable transition structure for monomer-based addition (**TS-11**, Figure 19) is less favorable by 4.4 kcal/mol using a monomer reference state, which appears to be a consequence of an inferior trajectory.

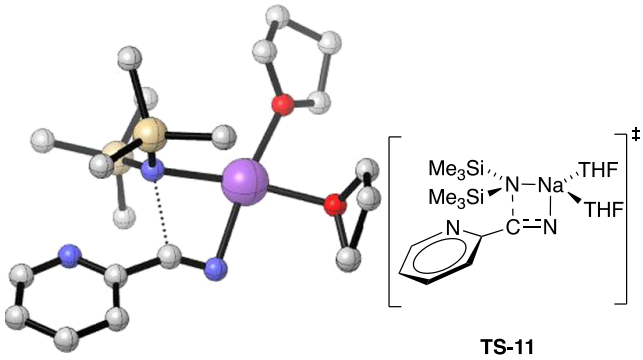

Figure 19. DFT-computed the transition structure TS-**11** for the unfavorable NaHMDS-monomer-based addition to nitrile **6**.

We would be remiss not to comment on the influence of 2,5-Me_2THF rather than pentane as the cosolvent for nitrile addition (curve C in Figure 16). It provided further evidence of cooperative solvation. While checking for polarity effects, we detected and subsequently documented cooperative monomer solvation, $(Me_3Si)_2NNa(THF)_x(Me_2THF)_y$, noted in eq 6. The details are obscured in Figure 16 by an overlaying THF concentration dependence. The complete suppression of the rate suggested that the mixed solvated monomers persisted as an unproductive side equilibrium at stunningly low THF concentrations. Indeed, this was caused by a steep temperature dependence of the deaggregation. The message for us is that 2,5-Me_2THF is a far better noncoordinating THF surrogate for lithium than for sodium.

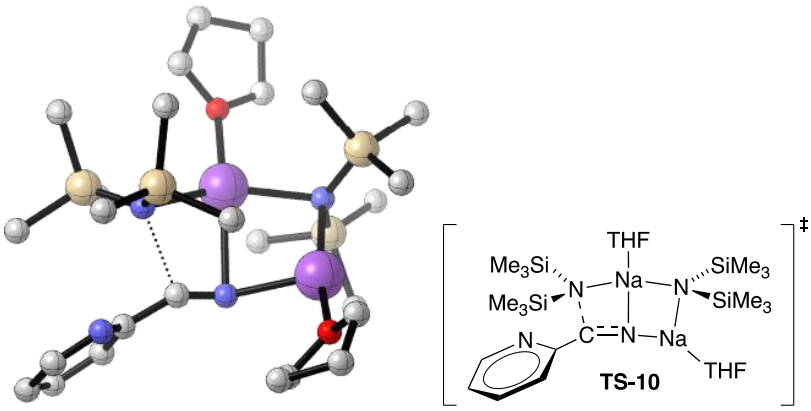

Figure 18. DFT-computed transition structure **TS-10** for the NaHMDS-dimer-based addition to nitrile **6**.

https://doi.org/10.1021/jacs.3c07317
J. Am. Chem. Soc. XXXX, XXX, XXX−XXX

Scheme 8. Summary of NaHMDS Mechanistic Studies in THF Solution

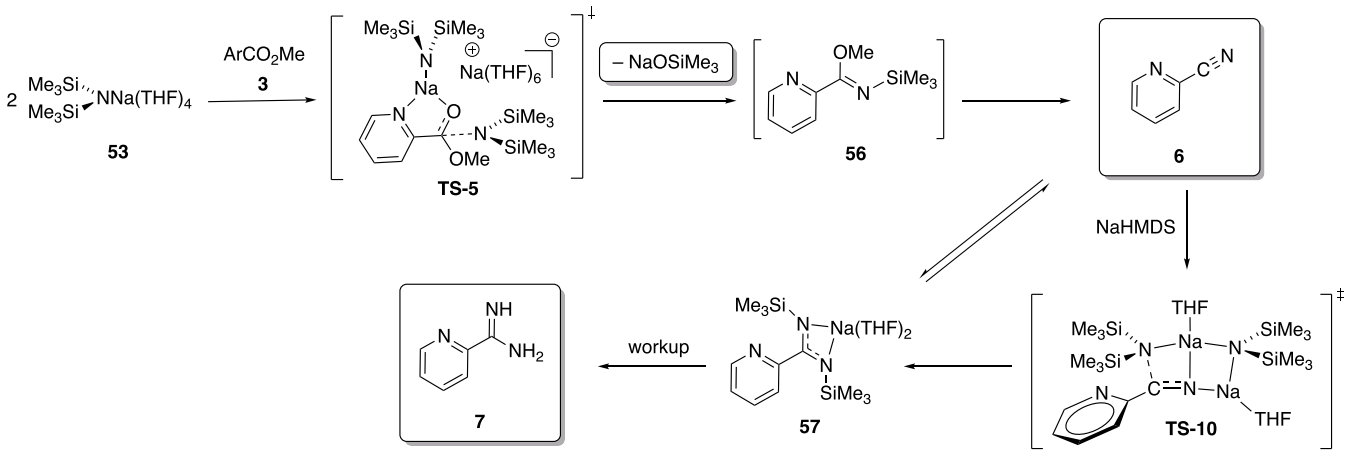

Scheme 9. Summary of NaHMDS Mechanistic Studies in DMEA Solution

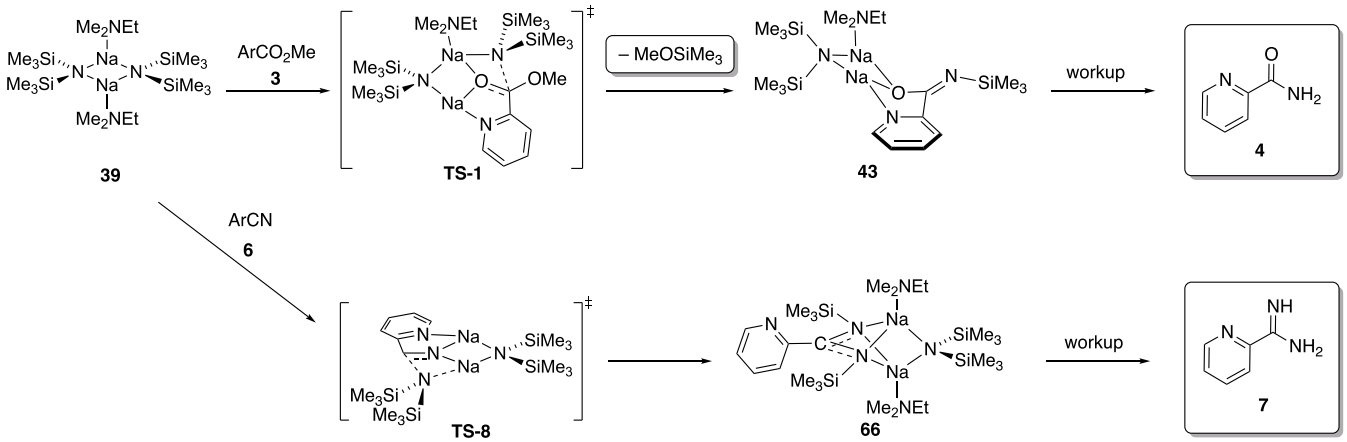

■ SUMMARY

The studies described above proved to be four discrete mechanistic studies in which the choice of solvent and conditions markedly influenced the outcome of the reactions. We offer an overview in which the results are grouped according to choice of THF or DMEA. This summary is organosodium centric; there is considerable organolsilicon chemistry (largely addressed computationally) that is left to the four parts described above. The arrows in Schemes 8 and 9 encompass many discrete steps including the organosilicon chemistry.

The THF results are summarized in Scheme 8. While NaHMDS in neat THF solution exists exclusively as tetrasolvated monomer **53**, it reacts with methyl-2-picolinate, **3**, via a dimer-based pathway in which triple-ion motif **TS-5** is invoked at the rate-limiting transition structure. The critical chemoselectivity stems from a post-rate-limiting extrusion of $NaOSiMe_3$ to form spectroscopically observable imino ether **56**, which reacts further to give nitrile **6** and sodium amidinate **57** en route to a high-yielding one-pot synthesis of amidine **7**. This ester-to-amidine conversion seems potentially important synthetically. Addition of NaHMDS to nitrile **6** is also dimer-based as depicted in computationally viable transition structure **TS-10**. The dominance of dimer-based reactivity under conditions affording *monomeric* NaHMDS should pique the interest of those interested in mechanistic alkali metal chemistry.

The chemistry of NaHMDS in poorly coordinating DMEA[7b] (Scheme 9) shows some parallels with the results in THF, but the differences are consequential. Although we do not consider a dimeric NaHMDS to be the proximate cause of dimer-based reactivity − many if not most monomer-based organoalkali metal reactions emanate from aggregates − the dominance of a dimer-based transition structure, **TS-1**, leading to observable mixed aggregate **43** aligns with previous studies of both LiHMDS and NaHMDS in DMEA.[7c,S4] In contrast to THF, however, a critical post-rate-limiting extrusion of $MeOSiMe_3$ rather than $NaOSiMe_3$ dictates the chemoselective formation of carboxamide **4**. Observable mixed aggregate **50** is robust but finds a path to **66** over a month at 25 °C. Although this is clearly an inferior route to amidine **7** we examined the addition to nitrile **6** and, once again, uncovered dimer-based chemistry via an unsolvated transition structure, **TS-8**.

■ CONCLUSIONS

While casting about for case studies to investigate solvent-structure−reactivity relationships in NaHMDS, we happened across several potentially useful reactions that are poorly represented in the literature and provided mechanistic insights that were wholly unexpected. The potential utility stems from C−N bond formation directly from aryl methyl esters, bypassing more activated forms. For us, however, they provided clean examples illustrating the role of solvation and aggregation in the chemistry of sodium amides in general and

https://doi.org/10.1021/jacs.3c07317
J. Am. Chem. Soc. XXXX, XXX, XXX−XXX

NaHMDS in particular. The NaHMDS itself serves as a preface to ongoing studies of sodium alkyl(trimethylsilyl) amides with potentially greater utility as strong bases and for C−N bond-forming reactions.

The dimer- and mixed dimer-based reactivity has precedent,[7c,36] but the total dominance of aggregate-based reactivity still came as a surprise. From a mechanistically tactical perspective, the work underscores both the power of ^{29}Si−^{15}N coupling to determine solution structures and the general merits of ^{29}Si NMR spectroscopy. (We asserted previously that ^{29}Si NMR spectroscopy is underutilized by those outside the organosilicon community.) We offer a final caveat to those who might be tempted to probe primary- vs secondary-shell solvation by using 2,5-Me$_2$THF as a polar, noncoordinating cosolvent. Despite its success in organolithium chemistry, the larger sodium ion may call for the more expensive 2,2,5,5-Me$_4$THF. On the truism that an effect is either sterics or electronics, ours' and others' experience with metal ion solvation is that sterics dominates.[55]

■ EXPERIMENTAL SECTION

Reagents and Solvents. NaHMDS and [^{15}N]NaHMDS were prepared as white crystalline solids.[7b] Toluene, hexanes, THF, MTBE, cyclopentane, 2,5-Me$_2$THF, and HMPA were distilled from blue or purple solutions containing sodium benzophenone ketyl. All substrates and products in Table 1 are commercially available.[31,32]

General Procedure A: Picolinamide 4. Solid sodium hexamethyldisilazide (NaHMDS, 165 mg, 0.9 mmol) was dissolved in 2.0 mL of DMEA at 25 °C. Two mL of the NaHMDS solution was added to a dry 5 mL Kimble vial equipped with a magnetic stir bar. Methyl-2-picolinate (**3**, 36 μL, 0.30 mmol) was then added to the reaction solution. The reaction mixture was stirred at 25 °C for 0.3 h. DI water (1 mL) was added, and the resulting biphasic mixture was partitioned between water (1 mL) and ethyl ether (2 mL). The aqueous layer was separated and extracted further with three 2 mL portions of ethyl ether. The combined organic layers were dried over anhydrous magnesium sulfate and then concentrated. Purification of the residue by flash column chromatography (80% ethyl acetate in hexanes) afforded picolinamide **4** as a white solid. ^{1}H NMR (500 MHz, CDCl3) δ 8.56 (d, J = 4.6 Hz, 1H), 8.20 (d, J = 7.8 Hz, 1H), 7.89 (s, 1H), 7.84 (td, J = 7.7, 1.8 Hz, 1H), 7.43 (dd, J = 7.6, 4.8 Hz, 1H), 6.23 (s, 1H). ^{13}C{^{1}H} NMR (126 MHz, CDCl$_3$) δ: 166.99, 145.59, 148.32, 137.31, 126.47, 122.44. HRMS (DART) Calc. for $C_6H_6N_2O$ (M + H$^+$): 123.04746; found: 123.05493.

General Procedure B: Amidine 7. Solid sodium hexamethyldisilazide (NaHMDS, 165 mg, 0.9 mmol) was dissolved in 1.5 mL of THF at 25 °C. 1.5 mL of the NaHMDS solution was added to a dry 5 mL Kimble vial equipped with a magnetic stir bar. Methyl picolinate (**3**, 36 μL, 0.30 mmol) was then added to the reaction solution. The reaction mixture was stirred at 50 °C for 0.3 h. DI water (1 mL) was then added. 2 M HCl aqueous solution was added to adjust pH = 1, which then was stirred at 25 °C for 1 h. Saturated NaOH solution was added until pH = 12, and the mixture was partitioned between water (1 mL) and chloroform (4 mL). The aqueous layer was separated and extracted further with three 4 mL portions of chloroform. The combined organic layers were dried over anhydrous magnesium sulfate and then concentrated to afford amidine **7** as a yellow oil. ^{1}H NMR (500 MHz, CDCl3) δ 8.56 (m, 1H), 8.11 (d, J = 7.9 Hz, 1H), 7.78 (td, J = 7.7, 1.8 Hz, 1H), 7.35 (dd, J = 7.5, 4.9 Hz, 1H), 5.94 (s, 3H). ^{13}C{^{1}H} NMR (126 MHz, CDCl$_3$) δ: 161.06, 150.79, 148.35, 137.03, 125.21, 120.81. HRMS (DART) Calc. for $C_6H_7N_3$ (M + H$^+$): 122.06345; found: 122.07097.

NMR Spectroscopic Analyses. An NMR tube fitted with a double-septum under vacuum was flame-dried on a Schlenk line and allowed to passively cool to room temperature, backfilled with argon, and placed in a dry ice/acetone cooling bath. Individual stock solutions of the substrate and NaHMDS or [^{15}N]NaHMDS were prepared at room temperature. The appropriate amounts of the substrate, NaHMDS, solvent, and cosolvent were added sequentially to the tube cooled to −78 °C via a gastight syringe. The tube was flame-sealed under a partial vacuum while cold to minimize evaporation in some cases and left unsealed for incremental additions. The tubes were mixed with a vortex mixer for approximately 10 s to minimize warming. Standard ^{1}H, ^{13}C, and ^{29}Si direct detection spectra were recorded at 500, 125.79, and 99.36 MHz, respectively, and referenced to Me$_4$Si (0.0 ppm). Integration of the NMR signals was determined using the line-fitting method included in MNova (Mestrelab research S.L.).

Rate Studies. IR spectra were recorded with an in situ IR spectrometer fitted with a 30-bounce, silicon-tipped probe. The spectra were acquired at a gain of 1 and a resolution of 4 cm^{-1}. All tracked reactions were conducted under a positive flow of argon from a Schlenk line. A representative reaction was carried out as follows: The IR probe was inserted through a Teflon adapter and an O-ring seal into an oven-dried, cylindrical flask fitted with a magnetic stir bar and a T-joint. The T-joint was capped with a septum for injections and an argon line. After evacuation under full vacuum, heating, and flushing with argon, the flask was charged with the solvent mixtures of our choice (toluene, DMEA, THF, 2,5-Me$_2$THF, and 2,2,5,5-Me$_4$THF) and cooled to −78 °C in a dry ice−acetone bath. A set of 256 baseline scans were collected, and IR spectra were recorded every 15 s from 30 scans. The reaction vessel was charged with stock solutions of NaHMDS and additional cosolvent through the septum. One set of scans was collected before the addition of substrate through the septum, and the baseline is zeroed. The substrate was added neat or in highly concentrated solutions and was tracked to completion (1731 cm^{-1} for **7**, for example). The spectrometer was configured to collect spectra every 5 s from 16 scans. The reaction was tracked over 3−5 half-lives monitoring the disappearance of the starting material and the appearance of the product. The former was used for the rate studies.

Density Functional Theory (DFT) Computations. All DFT calculations were carried out using Gaussian 16.[29] Prompted by a recent benchmarking of modern density functionals, all calculations were conducted at the M06-2X level of theory.[30a−c] A pruned (99,590) integration grid (equivalent to Gaussian's "UltraFine" option) was used for all calculations. The Ahlrichs basis set def2-svp was used for geometry optimizations and the expanded def2-tsvp basis set for single-point energy calculations.[30d] Ball-and-stick models were rendered using CYLview 1.0b.[30e] A large number of DFT-computed energies are archived in the Supporting Information.

■ ASSOCIATED CONTENT

Supporting Information

The Supporting Information is available free of charge at https://pubs.acs.org/doi/10.1021/jacs.3c07317.

Synthetic and experimental procedures, ^{1}H and ^{29}Si NMR spectroscopic, rate, and computational data (PDF)

■ AUTHOR INFORMATION

Corresponding Author

David B. Collum − *Department of Chemistry and Chemical Biology, Baker Laboratory, Cornell University, Ithaca, New York 14853-1301, United States;* orcid.org/0000-0001-6065-1655; Email: dbc6@cornell.edu

Author

Qiulin You − *Department of Chemistry and Chemical Biology, Baker Laboratory, Cornell University, Ithaca, New York 14853-1301, United States*

Complete contact information is available at: https://pubs.acs.org/10.1021/jacs.3c07317

https://doi.org/10.1021/jacs.3c07317
J. Am. Chem. Soc. XXXX, XXX, XXX−XXX

Notes

The authors declare no competing financial interest.

■ ACKNOWLEDGMENTS

The authors thank the National Institutes of Health (GM131713) for support.

■ REFERENCES

(1) (a) Mulvey, R. E.; Robertson, S. D. Synthetically Important Alkali-Metal Utility Amides: Lithium, Sodium, and Potassium Hexamethyldisilazides, Diisopropylamides, and Tetramethylpiperidides. *Angew. Chem., Int. Ed.* **2013**, *52*, 11470. (b) Robertson, S. D.; Uzelac, M.; Mulvey, R. E. Alkali-Metal-Mediated Synergistic Effects in Polar Main Group Organometallic Chemistry. *Chem. Rev.* **2019**, *119*, 8332. (c) McLellan, R.; Uzelac, M.; Bole, L. J.; Gil-Negrete, J. M.; Armstrong, D. R.; Kennedy, A. R.; Mulvey, R. E.; Hevia, E. Alkali Metal Effects in Trans-Metal-Trapping (TMT): Comparing LiTMP with NaTMP in Cooperative MTMP/Ga-$(CH_2SiMe_3)_3$ Metalation Reactions. *Synthesis* **2019**, *51*, 1207. (d) Garden, J. A.; Armstrong, D. R.; Clegg, W.; Garcia-Alvarez, J.; Hevia, E.; Kennedy, A. R.; Mulvey, R. E.; Robertson, S. D.; Russo, L. Donor-Activated Lithiation and Sodiation of Trifluoromethylbenzene: Structural, Spectroscopic, and Theoretical Insights. *Organometallics* **2013**, *32*, 5481. (e) Wong, H. N. C. Is Sodium Finally Coming of Age? *Nat. Catal.* **2019**, *2*, 282. (f) Lochmann, L.; Janata, M. 50 Years of Superbases Made from Organolithium Compounds and Heavier Alkali Metal Alkoxides. *Open Chem.* **2014**, *12*, 537. (g) Seyferth, D. Alkyl and Aryl Derivatives of the Alkali Metals: Strong Bases and Reactive Nucleophiles. 2. Wilhelm Schlenk's Organoalkali-Metal Chemistry. The Metal Displacement and the Transmetalation Reactions. Metalation of Weakly Acidic Hydrocarbons. Superbases. *Organometallics* **2009**, *28*, 2. (h) Davison, N.; Lu, E. The quest for Organo-Alkali Metal Monomers: Unscrambling the Structure−Reactivity Relationship. *Dalton Trans.* **2023**, *52*, 8172.

(2) Woltornist, R. A.; Ma, Y.; Algera, R. F.; Zhou, Y.; Zhang, Z.; Collum, D. B. Structure, Reactivity, and Synthetic Applications of Sodium Diisopropylamide. *Synthesis* **2020**, *52*, 1478.

(3) For a recent studies of illustrating the synthetic potential of organosodium chemistry, see: (a) Gentner, T. X.; Mulvey, R. E. Alkali-Metal Mediation: Diversity of Applications in Main-Group Organometallic Chemistry. *Angew. Chem., Int. Ed.* **2021**, *60*, 9247. (b) Anderson, D. E.; Tortajada, A.; Hevia, E. Highly Reactive Hydrocarbon Soluble Alkylsodium Reagents for Benzylic Aroylation of Toluenes Using Weinreb Amides. *Angew. Chem., Int. Ed.* **2023**, *62*, No. e202218498, DOI: 10.1002/anie.202218498. (c) Harenberg, J. H.; Reddy, A.; Karaghiosoff, K.; Knochel, P. Continuous Flow Preparation of Benzylic Sodium Organometallics. *Angew. Chem., Int. Ed.* **2022**, *61*, No. e202203807. (d) Davison, N.; McMullin, C. L.; Zhang, L.; Hu, S.-X.; Waddell, P. G.; Wills, C.; Dixon, C.; Lu, E. Li vs Na: Divergent Reaction Patterns between Organolithium and Organosodium Complexes and Ligand-Catalyzed Ketone/Aldehyde Methylenation. *J. Am. Chem. Soc.* **2023**, *145*, 6562. (e) De, P. B.; Asako, S.; Ilies, L. Recent Advances in the Use of Sodium Dispersion for Organic Synthesis. *Synthesis* **2021**, *53*, 3180.

(4) Ma, Y.; Lui, N. M.; Keresztes, I.; Woltornist, R. A.; Collum, D. B. Sodium Isopropyl(trimethylsilyl)amide (NaPTA): A Stable and Highly Soluble Lithium Diisopropylamide Mimic. *J. Org. Chem.* **2022**, *87*, 14223.

(5) Watson, B. T.; Lebel, H. Sodium Hexamethyldisilazide. In *e-EROS Encyclopedia of Reagents for Organic Synthesis*; John Wiley & Sons: New York, 2005; pp 1−10.

(6) (a) Driess, M.; Pritzkow, H.; Skipinski, M.; Winkler, U. Synthesis and Solid State Structures of Sterically Congested Sodium and Cesium Silyl(fluorosilyl)phosphanide Aggregates and Structural Characterization of the Trimeric Sodium Bis(trimethylsilyl)amide. *Organometallics* **1997**, *16*, 5108. (b) Kennedy, A. R.; Mulvey, R. E.; O'Hara, C. T.; Robertson, S. D.; Robertson, G. M. Catena-Poly[Sodium-μ_2-(*N,N,N′,N′*- Tetramethylethane-1,2-Diamine)-k^2-*N,N′*-Sodium- Bis[μ_2-Bis(Trimethylsilyl)Azanido-k^2 *N:N*]]. *Acta Crystallogr., Sect. E* **2012**, *68*, m1468. (c) Schüler, P.; Görls, H.; Westerhausen, M.; Kriec, S. Bis(trimethylsilyl)amide Complexes of s-Block Metals with Bidentate Ether and Amine Ligands. *Dalton Trans.* **2019**, *48*, 8966. (d) Ojeda-Amador, A. I.; Martínez-Martínez, A. J.; Kennedy, A. R.; Armstrong, D. R.; O'Hara, C. T. Monodentate Coordination of the Normally Chelating Chiral Diamine (*R,R*)-TMCDA. *Chem. Commun.* **2017**, *53*, 324. (e) Sarazin, Y.; Coles, S. J.; Hughes, D. L.; Hursthouse, M. B.; Bochmann, M. Cationic Brønsted Acids for the Preparation of Sn(IV) Salts: Synthesis and Characterisation of $[Ph_3Sn(OEt_2)][H_2N\{B(C_6F_5)_3\}_2]$, $[Sn(NMe_2)_3(HNMe_2)_2][B(C_6F_5)_4]$ and $[Me_3Sn(HNMe_2)_2][B(C_6F_5)_4]$. *Eur. J. Inorg. Chem.* **2006**, *2006*, 3211. (f) Karl, M.; Seybert, G.; Massa, W.; Harms, K.; Agarwal, S.; Maleika, R.; Stelter, W.; Greiner, A.; Neumüller, W. H.; Dehnicke, K. Amidometallate von Seltenerdelementen. Synthese Und Kristallstrukturen von $[Na(12\text{-Krone-}4)_2][M\{N(SiMe_3)_2\}_3(OSiMe_3)]$ (M = Sm, Yb), $[Na(THF)_3Sm\{N(SiMe_3)_2\}_3(C{\equiv}C\text{-Ph})]$, $[Na(THF)_6][Lu_2(\mu\text{-}NH_2)(\mu\text{-}NSiMe_3)\{N(SiMe_3)_2\}_4]$ Sowie von $[NaN(SiMe_3)_2(THF)]_2$. *Z. Anorg. Allg. Chem.* **1999**, *625*, 1301. (g) Neufeld, R.; Michel, R.; Herbst-Irmer, R.; Schöne, R.; Stalke, D. Introducing a Hydrogen-Bond Donor into a Weakly Nucleophilic Brønsted Base: Alkali Metal Hexamethyldisilazides (MHMDS, M = Li, Na, K, Rb, and Cs) with Ammonia. *Chem. − Eur. J.* **2016**, *22*, 12340. (h) Edelmann, F. T.; Pauer, F.; Wedler, M.; Stalke, D. Preparation and Structural Characterization of Dioxane Coordinated Alkali Metal Bis(Trimethylsilyl)Amides. *Inorg. Chem.* **1992**, *31*, 4143. (i) Also, see reference 10a.

(7) (a) Woltornist, R. A.; Collum, D. B. Sodium Hexamethyldisilazide: Using $^{15}N-^{29}Si$ Scalar Coupling to Determine Aggregation and Solvation States. *J. Am. Chem. Soc.* **2020**, *142*, 6852. (b) Woltornist, R. A.; Collum, D. B. Aggregation and Solvation of Sodium Hexamethyldisilazide: Across the Solvent Spectrum. *J. Org. Chem.* **2021**, *86*, 2406. (c) Woltornist, R. A.; Collum, D. B. Ketone Enolization with Sodium Hexamethyldisilazide: Solvent- and Substrate-Dependent E−Z Selectivity and Affiliated Mechanisms. *J. Am. Chem. Soc.* **2021**, *143*, 17452.

(8) (a) Brown, D. G.; Boström, J. Analysis of Past and Present Synthetic Methodologies on Medicinal Chemistry: Where Have All the New Reactions Gone? *J. Med. Chem.* **2016**, *59*, 4443. (b) Guan, Y.; Lee, T.; Wang, K.; Yu, S.; McWilliams, C. J. S_NAr Regioselectivity Predictions: Machine Learning Triggering DFT Reaction Modeling through Statistical Threshold. *J. Chem. Inf. Model.* **2023**, *63*, 3751.

(9) (a) Harrington, A.; Tal-Gan, Y. The Importance of Amide Protons in Peptide Drug Development. *Future Med. Chem.* **2019**, *11*, 2759. (c) Kumari, S.; Carmona, A. V.; Tiwari, A. K.; Trippier, P. C. Amide Bond Bioisosteres: Strategies, Synthesis, and Successes. *J. Med. Chem.* **2020**, *63*, 12290.

(10) For a NaHMDS-sodium enolate mixed aggregates, see: (a) Williard, P. G.; Hintze, M. J. Mixed Aggregates: Crystal Structures of a Lithium Ketone Enolate/Lithium Amide and of a Sodium Ester Enolate/Sodium Amide. *J. Am. Chem. Soc.* **1990**, *112*, 8602. (b) Zhang, Z.; Collum, D. B. Structures and Reactivities of Sodiated Evans Enolates: Role of Solvation and Mixed Aggregation on the Stereochemistry and Mechanism of Alkylations. *J. Am. Chem. Soc.* **2019**, *141*, 388. (c) Ojeda-Amador, A. I.; Martinez-Martinez, A. J.; Kennedy, A. R.; O'Hara, C. T. Synthetic and Structural Studies of Mixed Sodium bis(Trimethylsilyl) Amide/Sodium Halide Aggregates in the Presence of η^2-*N,N*-, η^3-*N,N,N/N,O,N*-, and η^4-*N,N,N,N*-Donor Ligands. *Inorg. Chem.* **2015**, *54*, 9833. (d) Knapp, C.; Lork, E.; Borrmann, T.; Stohrer, W.-D.; Mews, R. Versuche Zur Darstellung Vont-$BuCN_5S_3$ Und Die Unerwartete Isolierung Einer Kovalenten Modifikation von Tetraschwefelpentastickstoff-Chlorid S_4N_5Cl. *Z. Anorg. Allg. Chem.* **2005**, *631*, 1885. (e) Clark, N. M.; García-Álvarez, P.; Kennedy, A. R.; O'Hara, C. T.; Robertson, G. M. Reactions of (−)-Sparteine with Alkali Metal HMDS Complexes: Conventional Meets the Unconventional. *Chem. Commun.* **2009**, *39*, 5835. (f) Williard, P. G.; Nichols, M. A. Structural Characterization of Mixed Alkali Metal Bis(trimethylsilyl) Amide Bases. *J. Am. Chem. Soc.* **1991**, *113*, 9671.

https://doi.org/10.1021/jacs.3c07317
J. Am. Chem. Soc. XXXX, XXX, XXX−XXX

(11) We suspect that our failures and other failures to undergo 1,4-addition derive from a thermodynamic problem in which the reaction is endothermic. Products of cinnamate self-condensation of the *tert*-butylcinnamate dominated reaction contents. Ongoing studies of enolization with NaHMDS/THF-based enolizations suggest a delicately balanced equilibrium for some substrates (unpublished). 1,4-Addition to the malonate analog [PhCH = $C(CO_2Me)_2$, by contrast, are successful (unpublished). A 1,4-addition of LiHMDS to an unsaturated ester has been reported.[12]

(12) Rico, J. G. Synthesis of Novel *β*-Amino Acid Precursors: *β*-Amino-Hydrocoumarins as Unusual Aspartic Acid Mimetics Used in Fibrinogen Receptor Antagonists. *Tetrahedron Lett.* **1994**, *35*, 6599.

(13) (a) Krüger, C.; Rochow, E. G.; Wannagat, U. Uber die Reaktion von Natrium-bis-trimethylsilyl-amid mit Derivaten der Benzoesaure. *Chem. Ber.* **1963**, *96*, 2138. (b) Afifi, M. S.; El-Sayed, B. A. Spectroscopic Investigation of the Reaction Products Between the Sodium Salt of Hexamethyldisilazane and Ethyl Salicylate. Mass Spectra, Proton Magnetic Resonance and Infrared Analysis. *Egypt. J. Chem.* **1983**, *26*, 551.

(14) Hwu, J. R.; Hsu, C. H.; Wong, F. F.; Chung, C.-S.; Hakimelahi, G. H. Sodium Bis(trimethylsilyl)amide in the "One-Flask" Transformation of Aromatic Esters to Nitriles. *Synthesis* **1998**, *1998*, 329.

(15) (a) Abou-Elkhair, R. A. I.; Hassan, A. E. A.; Boykin, D. W.; Wilson, W. D. Lithium Hexamethyldisilazane Transformation of Transiently Protected 4-Aza/benzimidazole Nitriles to Amidines and Their Dimethyl Sulfoxide-Mediated Imidazole Ring Formation. *Org. Lett.* **2016**, *18*, 4714. (b) Alharbi, N.; Díaz-Moscoso, A.; Tizzard, G. J.; Coles, S. J.; Cook, M. J.; Cammidge, A. N. Improved Syntheses of meso-Aryl Tetrabenzotriazaporphyrins (TBTAPs). *Tetrahedron* **2014**, *70*, 7370.

(16) (a) Baumann, M.; Baxendale, I. R. A continuous flow synthesis and derivatization of 1,2,4-thiadiazoles. *Bioorg. Med. Chem.* **2017**, *25*, 6218 DOI: 10.1016/j.bmc.2017.01.022. (b) Dorsey, B. D.; Dugan, B. J.; Fowler, K. M.; Hudkins, R. L.; Mesaros, E. F.; Monck, N. J.; Morris, E. L.; Olowoye, I.; Ott, G. R.; Pave, G. A.; Roffey, J. R. A.; Soudy, C. N.; Zificsak, C. A.; Zulli, A. L. Preparation of Azaquinazoline Inhibitors of Atypical Protein Kinase C. WIPO Patent WO2015148597, 2015.

(17) Chen, J.; Xu, Z.; Wang, T.; Lyssikatos, J. P.; Ndubaku, C. O. A Versatile Annulation Route to Primary-Amino-Substituted Naphthyridine Esters. *Synlett* **2013**, *25*, 89.

(18) Guedira, N. E.; Beugelmans, R. Ambident Behavior of Ketone Enolate Anions in S_NAr Substitutions on Fluorobenzonitrile Substrates. *J. Org. Chem.* **1992**, *57*, 5577.

(19) Sun, K.; Sagisaka, K.; Peng, L.; Watanabe, H.; Xu, F.; Pawlak, R.; Meyer, E.; Okuda, Y.; Orita, A.; Kawai, S. Head-to-Tail Oligomerization by Silylene-Tethered Sonogashira Coupling on Ag(111). *Angew. Chem., Int. Ed.* **2021**, *60*, 19598.

(20) Li, G.; Ji, C.; Hong, X.; Szostak, M. Highly Chemoselective, Transition-Metal-Free Transamidation of Unactivated Amides and Direct Amidation of Alkyl Esters by N−C/O−C Cleavage. *J. Am. Chem. Soc.* **2019**, *141*, 11161.

(21) Hwu, J. R.; Das, A. R.; Chuang, K.-S.; Yang, C. W.; Chuang, S. H.; Huang, J. J.; Tsay, S.-C. 1,2-Eliminations in a Novel Reductive Coupling of Nitroarenes to Give Azoxy Arenes by Sodium Bis(trimethylsilyl)amide. *Org. Lett.* **2005**, *7*, 3211.

(22) For a discussion and leading references to the challenges of metalating nitroarenes, see: Nagaki, A.; Kim, H.; Yoshida, J.-i. Nitro-Substituted Aryl Lithium Compounds in Microreactor Synthesis: Switch Between Kinetic and Thermodynamic Control. *Angew. Chem., Int. Ed.* **2009**, *48*, 8063.

(23) For a similar trimethylsilyl transfer that occurs when benzyne is trapped by metal silazides, see: Ikawa, T.; Masuda, S.; Akai, S. One-Pot Generation of Benzynes from Phenols: Formation of Primary Anilines by the Deoxyamination of Phenols. *Chem. − Eur. J.* **2020**, *26*, 4320.

(24) Schnürch, M.; Spina, M.; Khan, A. F.; Mihovilovic, M. D.; Stanetty, P. Halogen Dance Reactions—A Review. *Chem. Soc. Rev.* **2007**, *36*, 1046.

(25) Estel, L.; Marsais, F.; Queguiner, G. Metalation/SRN1 Coupling in Heterocyclic Synthesis. A Convenient Methodology for Ring Functionalization. *J. Org. Chem.* **1988**, *53*, 2740.

(26) Kadambar, V. K.; Bachu, S.; Reddy, M. R.; Torlikonda, V.; Manjunatha, S. G.; Ramasubramanian, S.; Nambiar, S.; Howell, G. B.; Withnall, J.; Murugan, A. Regioselective Synthesis of 1,2-Amino-alcohols from Epoxides and Chlorohydrins. *Tetrahedron Lett.* **2012**, *53*, 5739.

(27) (a) Wang, J.; Rosingana, M.; Discordia, R. P.; Soundararajan, N.; Polniaszek, R. Aminolysis of Esters or Lactones Promoted by NaHMDS - A General and Efficient Method for the Preparation of N-Aryl Amides. *Synlett* **2001**, *2001*, 1485. (b) Jones, C. D.; Bunyard, P.; Pitt, G.; Byrne, L.; Pesnot, T.; Guisot, N. Heterocyclylamino-substituted Triazoles as Modulators of rho-Associated Protein Kinase. WIPO Patent WO2019145729, 2019.

(28) Several general-purpose reviews on determining reaction mechanism: (a) Meek, S. J.; Pitman, C. L.; Miller, A. J. M. Deducing Reaction Mechanism: A Guide for Students, Researchers, and Instructors. *J. Chem. Educ.* **2016**, *93*, 275. (b) Simmons, E. M.; Hartwig, J. F. On the Interpretation of Deuterium Kinetic Isotope Effects in C−H Bond Functionalizations by Transition Metal Complexes. *Angew. Chem., Int. Ed.* **2012**, *51*, 3066. (c) Collum, D. B.; McNeil, A. J.; Ramírez, A. Lithium Diisopropylamide: Solution Kinetics and Implications for Organic Synthesis. *Angew. Chem., Int. Ed.* **2007**, *46*, 3002. (d) Algera, R. F.; Gupta, L.; Hoepker, A. C.; Liang, J.; Ma, Y.; Singh, K. J.; Collum, D. B. Lithium Diisopropylamide: Non-Equilibrium Kinetics and Lessons Learned about Rate Limitation. *J. Org. Chem.* **2017**, *82*, 4513.

(29) Frisch, M. J.; Trucks, G. W.; Schlegel, H. B.; Scuseria, G. E.; Robb, M. A.; Cheeseman, J. R.; Scalmani, G.; Barone, V.; Petersson, G. A.; Nakatsuji, H.; Li, X.; Caricato, M.; Marenich, A. V.; Bloino, J.; Janesko, B. G.; Gomperts, R.; Mennucci, B.; Hratchian, H. P.; Ortiz, J. V.; Izmaylov, A. F.; Sonnenberg, J. L.; Williams-Young, D.; Ding, F.; Lipparini, F.; Egidi, F.; Goings, J.; Peng, B.; Petrone, A.; Henderson, T.; Ranasinghe, D.; Zakrzewski, V. G.; Gao, J.; Rega, N.; Zheng, G.; Liang, W.; Hada, M.; Ehara, M.; Toyota, K.; Fukuda, R.; Hasegawa, J.; Ishida, M.; Nakajima, T.; Honda, Y.; Kitao, O.; Nakai, H.; Vreven, T.; Throssell, K.; Montgomery, J. A., Jr.; Peralta, J. E.; Ogliaro, F.; Bearpark, M. J.; Heyd, J. J.; Brothers, E. N.; Kudin, K. N.; Staroverov, V. N.; Keith, T. A.; Kobayashi, R.; Normand, J.; Raghavachari, K.; Rendell, A. P.; Burant, J. C.; Iyengar, S. S.; Tomasi, J.; Cossi, M.; Millam, J. M.; Klene, M.; Adamo, C.; Cammi, R.; Ochterski, J. W.; Martin, R. L.; Morokuma, K.; Farkas, O.; Foresman, J. B.; Fox, D. J. *Gaussian 16*, revision C.01; Gaussian, Inc.: Wallingford, CT, 2016.

(30) (a) Mardirossian, N.; Head-Gordon, M. Thirty Years of Density Functional Theory in Computational Chemistry: An Overview and Extensive Assessment of 200 Density Functionals. *Mol. Phys.* **2017**, *115*, 2315. (b) Wang, Y.; Verma, P.; Jin, X.; Truhlar, D. G.; He, X. Revised M06 Density Functional for Main-Group and Transition-Metal Chemistry. *Proc. Natl. Acad. Sci. U.S.A.* **2018**, *115*, 10257. (c) Zhao, Y.; Truhlar, D. G. The M06 Suite of Density Functionals for Main Group Thermochemistry, Thermochemical Kinetics, Noncovalent Interactions, Excited States, and Transition Elements: Two New Functionals and Systematic Testing of Four M06-Class Functionals and 12 Other Function. *Theor. Chem. Acc.* **2008**, *120*, 215. (d) Weigend, F.; Ahlrichs, R. Balanced Basis Sets of Split Valence, Triple Zeta Valence and Quadruple Zeta Valence Quality for H to Rn: Design and Assessment of Accuracy. *Phys. Chem. Chem. Phys.* **2005**, *7*, 3297. (e) Legault, C. Y. *CYLview, 1.0b*; Université de Sherbrooke, 2009 http://www.cylview.org.

(31) Chen, J.; Xia, Y.; Lee, S. Transamidation for the Synthesis of Primary Amides at Room Temperature. *Org. Lett.* **2020**, *22*, 3504.

(32) Jones, A. C.; Williams, M. T. J.; Morrill, L. C.; Browne, D. L. Mechanical Activation of Zero-Valent Metal Reductants for Nickel-Catalyzed Cross-Electrophile Coupling. *ACS Catal.* **2022**, *12*, 13681.

(33) Amidine **31** (Scheme 5) can be isolated after a month at 25 °C.

(34) The computations use the Gaussian standard state of 1.0 atm. If the THF concentration is corrected to neat THF (approximately 13 M), each solvation step benefits from approximately 2.0 kcal/mol of

https://doi.org/10.1021/jacs.3c07317
J. Am. Chem. Soc. XXXX, XXX, XXX−XXX

additional stabilization at − 78 °C (195 K) Pratt, L. M.; Merry, S.; Nguyen, S. C.; Quan, P.; Thanh, B. T. A Computational Study of Halomethyllithium Carbenoid Mixed Aggregates with Lithium Halides and Lithium Methoxide. *Tetrahedron* **2006**, *62*, 10821.

(35) Rein, A. J.; Donahue, S. M.; Pavlosky, M. A. In Situ FTIR Reaction Analysis of Pharmaceutical-Related Chemistry and Processes. *Curr. Opin. Drug Discovery Dev.* **2000**, *3*, 734.

(36) For leading references to open-dimer-based mechanisms, mechanisms that appear to involve monomer-to-dimer preaggregation, triple ion-based mechanisms, and solvation of sodium cation, see ref 7c and references cited therein.

(37) Intrinsic reaction coordinate (IRC) calculations are defined as "the minimum energy reaction pathway (MERP) in mass-weighted cartesian coordinates between the transition state of a reaction and its reactants and products." They show the minima preceding and following transition state.

(38) For a crystal structure of a lithium amidinate akin to **30** characterized crystallographically and excellent references to the applications of such amidinates, see: Aharonovich, S.; Kapon, M.; Botoshanski, M.; Eisen, M. S. *N,N′*-Bis-Silylated Lithium Aryl Amidinates: Synthesis, Characterization, and the Gradual Transition of Coordination Mode from σ Toward π Originated by Crystal Packing Interactions. *Organometallics* **2008**, *27*, 1869.

(39) Verstuyft, A. W.; Nelson, J. H.; Cary, L. W. Utility of Virtual Coupling in the Carbon-13 {proton} Nuclear Magnetic Resonance Spectra of Bis-phosphite Complexes of Palladium and Platinum. Algebraic Cancellation of Spin-Spin Coupling. *Inorg. Chem.* **1976**, *15*, 732.

(40) Reich, H. J.; Dykstra, R. R. Solution Structure of Lithium Benzeneselenolate and Lithium Diphenylphosphide: NMR Identification of Cyclic Dimers and Mixed Dimers. *Organometallics* **1994**, *13*, 4578.

(41) Perrin, C. L.; Shrinidhi, A.; Burke, K. D. Isotopic-Perturbation NMR Study of Hydrogen-Bond Symmetry in Solution: Temperature Dependence and Comparison of OHO and ODO Hydrogen Bonds. *J. Am. Chem. Soc.* **2019**, *141*, 17278.

(42) Edwards, J. O.; Greene, E. F.; Ross, J. From Stoichiometry and Rate Law to Mechanism. *J. Chem. Educ.* **1968**, *45*, 381.

(43) Ashby, E. C.; Dobbs, F. R.; Hopkins, H. P., Jr. Composition of Complex Aluminum Hydrides and Borohydrides, as Inferred from Conductance, Molecular Association, and Spectroscopic Studies. *J. Am. Chem. Soc.* **1973**, *95*, 2823.

(44) Me_4THF binds to NaHMDS, CsHMDS, and RbHMDS at least reluctantly as evidenced by X-ray crystal structures of the disolvated dimers showing significant distortions when compared with the THF solvates. LiHMDS crystallizes from Me_4THF as a solvent-free tetramer, although there is evidence it binds weakly in solution.[45] Krieck, S.; Schüler, P.; Görls, H.; Westerhausen, M. Straightforward Synthesis of Rubidium Bis(trimethylsilyl)amide and Complexes of the Alkali Metal Bis(trimethylsilyl)amides with Weakly Coordinating 2,2,5,5- Tetramethyltetrahydrofuran. *Dalton Trans.* **2018**, *47*, 12562.

(45) Lucht, B. L.; Collum, D. B. Ethereal Solvation of Lithium Hexamethyldisilazide (LiHMDS): Unexpected Relationships of Solvation Number, Solvation Energy, and Aggregation State. *J. Am. Chem. Soc.* **1995**, *117*, 9863.

(46) (a) Bates, R. B.; Kroposki, L. M.; Potter, D. E. Cycloreversions of Anions from Tetrahydrofurans. A Convenient Synthesis of Lithium Enolates of Aldehydes. *J. Org. Chem.* **1972**, *37*, 560. (b) Byrne, F.; Forier, B.; Bossaert, G.; Hoebers, C.; Farmer, T. J.; Clark, J. H.; Hunt, A. J. 2,2,5,5-Tetramethyltetrahydrofuran (TMTHF): a Non-polar, Non-peroxide Forming Ether Replacement for Hazardous Hydrocarbon Solvents. *Green Chem.* **2017**, *19*, 3671.

(47) The dielectric constants of substituted tetrahydrofurans are slightly lower than THF. (a) Harada, Y.; Salomon, M.; Petrucci, S. Molecular Dynamics and Ionic Associations of Lithium Hexafluoroarsenate ($LiAsF_6$) in 4-Butyrolactone Mixtures with 2-Methyltetrahydrofuran. *J. Phys. Chem. A* **1985**, *89*, 2006. (b) Carvajal, C.; Tolle, K. J.; Smid, J.; Szwarc, M. Studies of Solvation Phenomena of Ions and Ion Pairs in Dimethoxyethane and Tetrahydrofuran. *J. Am. Chem. Soc.* **1965**, *87*, 5548.

(48) The Principle of Detailed Balance asserts that individual equilibria within an ensemble of equilibria are maintained. It is particularly useful in understanding the complex equilibria observed in organolithium chemistry. Alberty, R. A. Principle of Detailed Balance in Kinetics. *J. Chem. Educ.* **2004**, *81*, 1206.

(49) Linder, T.; Sutherland, T. C.; Baumgartner, T. Extended 2,5-Diazaphosphole Oxides: Promising Electron-Acceptor Building Blocks for π-Conjugated Organic Materials. *Chem. − Eur. J.* **2010**, *16*, 7101.

(50) Substitution of the π-bound substrate in **43** with benzene is endothermic by 6.1 kcal/mol.

(51) The mathematics is in the Supporting Information of ref 7b.

(52) The order in THF cannot be determined from a fit with values of −4 through −6 all providing adequate fits to the data. The presumed value of −6 comes from the assigned solvation states of NaHMDS monomer as tetrasolvated,[7b] and transition structure **50** as a disolvate.

(53) A monomer-based *N*-to-*N′* silicon transfer analogous to that depicted in Figure 18 is substantially less favorable.

(54) (a) Zhao, P.; Collum, D. B. Ketone Enolization by Lithium Hexamethyldisilazide: Structural and Rate Studies of the Accelerating Effects of Trialkylamines. *J. Am. Chem. Soc.* **2003**, *125*, 14411. (b) Mack, K. A.; McClory, A.; Zhang, H.; Gosselin, F.; Collum, D. B. Lithium Hexamethyldisilazide-Mediated Enolization of Highly Substituted Aryl Ketones: Structural and Mechanistic Basis of the E/Z Selectivities. *J. Am. Chem. Soc.* **2017**, *139*, 12182.

(55) Su, C.; Guang, J.; Williard, P. G. Structures of Lithium *N*-Monosubstituted Anilides: Trisolvated Monomer to Tetrasolvated Dimer. *J. Org. Chem.* **2014**, *79*, 1032.

https://doi.org/10.1021/jacs.3c07317
J. Am. Chem. Soc. XXXX, XXX, XXX−XXX